A Novel Rapid Host Cell Entry Pathway Determines Intracellular Fate of *Staphylococcus aureus*

Marcel Rühling[1], Fabio Schmelz[1], Kim Ulbrich[1], Fabian Schumacher[2], Julia Wolf[1], Maximilian Pfefferle[1], Magdalena Priester[1], Adriana Moldovan[1], Nadine Knoch[1], Andreas Iwanowitsch[1], Christian Kappe[3], Kerstin Paprotka[2], Burkhard Kleuser[2], Christoph Arenz[3], and Martin J. Fraunholz[1+]

[1]Chair of Microbiology, Julius-Maximilians-University Würzburg, Theodor-Boveri-Weg, 97074 Würzburg, Germany

[2]Institute of Pharmacy, Freie Universität Berlin, Königin-Luise-Straße 2+4, 14195 Berlin, Germany

[3]Institut for Chemistry, Humboldt Universität zu Berlin, Brook-Taylor-Str. 2, 12489 Berlin, Germany

[+]Corresponding author: martin.fraunholz@uni-wuerzburg.de

Abstract:

Staphylococcus aureus is an opportunistic pathogen causing severe diseases. Recently, *S. aureus* was recognized as intracellular pathogen, whereby the intracellular niche promotes immune evasion and antibiotic resistance. Interaction of *S. aureus* with versatile host cell receptors was described previously, suggesting that internalization of the pathogen can occur via several pathways. It remains elusive whether the pathway of internalization can affect the intracellular fate of the bacteria. Here, we identified a mechanism governing cellular uptake of *S. aureus* which relies on lysosomal Ca^{2+}, lysosomal exocytosis and occurs concurrently to other well-known entry pathways within the same host cell population. This internalization pathway is rapid and active within only few minutes after bacterial contact with host cells. Compared to slow bacterial internalization, the rapid pathway demonstrates altered phagosomal maturation as well as translocation of the pathogen to the host cytosol and ultimately results in different rates of intracellular bacterial replication and host cell death. We show that these alternative infection outcomes are caused by the mode of bacterial uptake.

Introduction

Sphingolipids are important components of eukaryotic membranes and also serve as bioactive signaling molecules (1). The most abundant sphingolipid, sphingomyelin (SM), resides in the extracellular leaflet of the plasma membrane and hence is exposed to the environment (2, 3). SM is a substrate for sphingomyelinases (SMases) that cleave off the phosphocholine head group to produce ceramide. Acid sphingomyelinase (ASM) is a lysosomal enzyme involved in recycling of SM (4, 5). Several studies demonstrated that ASM can be released by human cells either by Ca^{2+}-dependent liberation of lysosomal content via so called lysosomal exocytosis (6-8) or by channeling the enzyme through the Golgi secretory pathway (9, 10). Extracellular ASM is active on the plasma membrane, where it has important roles during repair of membrane wounds (6, 11) but has also been shown to act on the SM-containing low-density lipoprotein (12). The release of ASM through lysosomal exocytosis mediates host cell entry of several human pathogens (7, 8, 13-17).

Staphylococcus aureus is a Gram-positive human commensal that asymptomatically colonizes about one third of the human population (18). It is an opportunistic pathogen causing diseases ranging from soft tissue and skin infections (19) to lethal diseases (20, 21). *S. aureus* is notorious for acquiring antibiotic resistances thereby causing >100,000 annual deaths (22). The pathogen possesses intracellular virulence strategies (23, 24) which contribute to antibiotic resistance (25, 26) and immune evasion (27). Internalization of *S. aureus* by host cells is mediated by several adhesins on the staphylococcal surface that bind a plethora of receptors on the host cell plasma membrane (13, 28-38). For instance, staphylococcal fibronectin-binding proteins that form fibronectin bridges to $\alpha_5\beta_1$ integrins on host cells to initiate internalization (28) or clumping factor B which can interact with the host receptor annexin A2 (31).

After internalization, *S. aureus* resides within a phagosome-like compartment that matures by acquiring proteins associated with early and then late endosomes as well as lysosomes (39-41). In epithelial and endothelial cells, the bacteria translocate to the host cytosol ["phagosomal escape", (39, 42, 43)]. Phagosomal escape is mediated by so-called phenol-soluble modulins (42), which comprise a family of helical amphiphilic peptides and are transcriptionally controlled by the accessory gene regulator *agr*, a staphylococcal quorum sensing system (44). *S. aureus* replicates in the host cytosol and causes host cell death for example by expression of a cysteine protease. (45).

The mechanism of pathogen entry into host cells has been suggested to dictate the outcome of infections (46-49). For instance, phagosomes formed during natural internalization of *Brucella abortus* by macrophages exhibited different characteristics compared to phagosomes that were artificially generated by phorbol myristate acetate (49). The protozoan parasite *Toxoplasma gondii* actively invades its host cells. Phagosomes generated during this active invasion differed from those that were generated during Fc receptor-mediated uptake of antibody-coated parasites (48). Since previous observation connecting host cell entry and intracellular fate of pathogens were based on artificial induction of internalization, it is unclear whether pathogens can enter host cells within the same population via different naturally occurring mechanisms and if the entry route has a direct influence on the outcome of an intracellular infection.

Here, we describe the internalization of *S. aureus* by tissue cells via a rapid pathway taking place within minutes after contact between bacteria and host cell surface. This pathway requires nicotinic acid adenosine dinucleotide phosphate (NAADP)-dependent mobilization of lysosomal Ca^{2+}, followed by lysosomal exocytosis and thereby release of ASM. Since the rapid uptake is concurrent to previously described internalization pathways, it probably has been missed due to long infection times used in traditional infection protocols [e.g., (28, 31, 35, 36)].

S. aureus bacteria, which enter host cells of the same cell population via the rapid pathway, cause a distinct infection outcome with altered phagosome maturation, bacterial translocation to host cytosol and eventually host cell death when compared to bacteria that enter host cells at later time points during infection. Thus, the outcome of an infection is decided at the single cell level during bacterial uptake at

the host plasma membrane. Bacteria-containing phagosomes that were formed by the ASM-dependent rapid uptake pathway are delayed in their maturation and the bacteria do not escape these organelles efficiently, hence demonstrating a direct link between concurrently active modes of bacterial uptake and the resulting outcomes of intracellular *S. aureus* infection.

Results

S. aureus triggers lysosomal Ca^{2+} mobilization for host cell invasion

We previously showed that internalization of *S. aureus* by host cells is associated with cellular Ca^{2+} signaling (50). To validate these findings, we treated human microvascular endothelial cells (HuLEC, **Figure 1**, A) or HeLa (**Supp. Figure 1**, A) with the cell permeant Ca^{2+} chelator BAPTA-AM (51) to interfere with host cell Ca^{2+} signaling and subsequently infected the cells with *S. aureus*. We measured the number of internalized *S. aureus* and determined the invasion efficiency by normalizing bacteria numbers detected in treated samples to untreated controls (set to 100%). Invasion efficiency was reduced by BAPTA-AM in a concentration-dependent manner, indicating an involvement of Ca^{2+} in the host cell entry process of *S. aureus*.

The cytosolic Ca^{2+} levels, which are crucial for signaling processes, can be elevated by Ca^{2+} influx from the extracellular space. To test whether *S. aureus* internalization is mediated by Ca^{2+} influx, we measured invasion efficiency, in absence of Ca^{2+} from the cell culture medium (**Figure 1**, A and **Supp. Figure 1**, A). Internalization of *S. aureus* by host cells was not affected by absence of Ca^{2+} ("Ca^{2+}-free, 0 µM BAPTA-AM"), thereby excluding a Ca^{2+} influx as crucial for *S. aureus* host cell entry. The pore-forming staphylococcal α-toxin was shown to mediate Ca^{2+} influx into host cells (11). *S. aureus* invasion into host cells was largely independent of the production of α-toxin (**Supp. Figure 1**, B), which further supported that the internalization is independent from extracellular Ca^{2+}.

Since intracellular Ca^{2+} stores, such as the ER or lysosomes, can serve as alternative source of Ca^{2+} (52), we next blocked Ca^{2+} liberation either from the ER using 2-APB (53) or 8-Bromo-cyclic ADP ribose (8-Bromo-cADPR; (54)) or from lysosomes using *trans*-Ned19 (55). Interference with lysosomal but not ER Ca^{2+} release reduced internalization of *S. aureus* in HuLEC (**Figure 1**, B) or HeLa (**Supp. Figure 1**, C, D) at concentrations which do not affect bacterial viability (**Supp. Figure 1**, E and F).

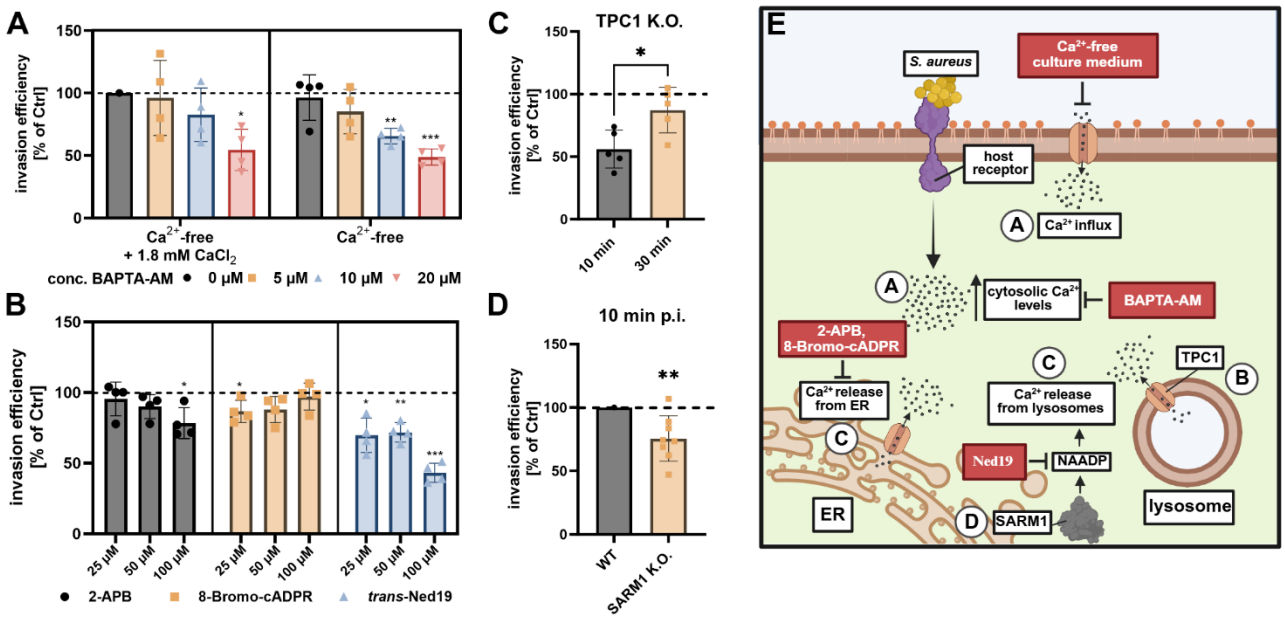

Figure 1 *S. aureus* invasion is dependent on Ca^{2+} liberation from lysosomal stores. Treatment with , BAPTA-AM (A, n≥4), *trans*-Ned19 (B, n≥4), but not 2-APB and 8-Bromo-cADPR (B, n≥4) reduce *S. aureus* internalization by host cells. Genetic ablation of TPC1 (C, n=5) and SARM1 (D, n=8) reduced invasion of *S.*

aureus 10 min p.i . HuLEC (A, B), HeLa WT (C, D), HeLa TPC1 K.O. (C) or HeLa SARM1 K.O. (D) cells were treated with the respective substance and were subsequently infected with *S. aureus* JE2 for 30 min if not indicated otherwise. Extracellular bacteria were removed by lysostaphin, and the number of intracellular bacteria was determined by CFU counting. Results were normalized to untreated controls to obtain invasion efficiency (in percent of control). (F) Scheme of host cell Ca^{2+} signaling and interfering agents. Letters indicate figure panels that supported the respective conclusion. Statistics: one sample t-test (A, B,D,), unpaired Student´s t-test (C). Bars represent means ± SD. *p≤0.05, **p≤0.01, ***p≤0.001, ****p≤0.0001.

Ned19 antagonizes NAADP, a second messenger that mediates opening of two pore channels (TPCs), which transport Ca^{2+} from the endo-lysosomal compartment into the cytosol (55). Hence, a HeLa cell pool depleted of TPC1 (**Supp. Figure 1***,* G) showed substantially reduced invasion when compared to wildtype HeLa cells. This was particularly pronounced after a 10 min infection pulse, suggesting that Ca^{2+}-dependent invasion is important early in infection (**Figure 1**, C).

CD38 is a well-known producer of NAADP in immune cells (56-58). Thus, we tested *S. aureus* invasion in HeLa cells treated with the specific CD38 inhibitor 78c, even though expression of CD38 in these cells is predicted to be very low (proteinatlas.org). We observed no effect on *S. aureus* invasion by CD38 inhibition (**Supp. Figure 1**, H). An alternative NAADP producer, with higher expression in our infection model, is *Sterile Alpha and TIR Motif Containing 1* [SARM1, (59)]. We measured a slightly decreased invasion efficiency 10 min p.i. in a cell pool lacking SARM1 when compared to wildtype cells (**Figure 1**, D; **Supp. Figure 1**, I), suggesting that SARM1 might be involved in NAADP production during internalization of *S. aureus* by host cells. However, there might be other enzymes that produce NAADP (60) during *S. aureus* infection.

Altogether, our findings show that interference with lysosomal Ca^{2+} mobilization limits *S. aureus* invasion particularly early in infection.

S. aureus invasion requires lysosomal exocytosis, ASM and its substrate sphingomyelin on the host cell surface

Since our data suggest that lysosomal Ca^{2+} release facilitates the internalization of *S. aureus* by host cells, we speculated that lysosomal exocytosis is involved in bacterial invasion. Lysosomal exocytosis is a Ca^{2+}-dependent process during which lysosomes fuse with the plasma membranes and release their content. The internalization of several human pathogens has been shown to depend on lysosomal exocytosis (8, 16, 61-63).

To visualize lysosomal exocytosis, we developed an assay that makes use of the split NanoLuc luciferase system [**Figure 2**, A; (64, 65)]. We here engineered HeLa cells to express the high-affinity NanoLuc peptide HiBiT between the signal peptide and the mature chain of lysosomal-associated membrane protein 1 (LAMP1). Transient localization of LAMP1 to the cell surface of mammalian cells is a hall mark for lysosomal exocytosis (66). To measure the release of the HiBiT-tagged LAMP1, we added LgBit together with the NanoLuc substrate Furimazine to the cell culture medium and measured luminescence of reconstituted NanoLuc in a microplate reader. Maximum luminescence was detected ~10-15 min upon starting the assay and decline afterwards, likely due to exhaustion of the luciferase substrate (**Figure 2**, B). Treatment with the Ca^{2+} ionophore ionomycin, a known activator of lysosomal exocytosis (11, 67), increased the luminescence, whereas Vacuolin-1, an inhibitor of lysosomal exocytosis (68), decreased luminescence when compared to an untreated control. Thus, we concluded that our assay successfully quantified exposure of LAMP1 on the host cell surface.

Next, we monitored LAMP1 surface levels during *S. aureus* infection. We assumed that ionomycin would trigger exocytosis of all "releasable" lysosomes. Hence, the detected luminescence signal during infection was scaled to an untreated control (=0 %) as well as ionomycin (=100%), to express LAMP1 surface levels as percentage of all "releasable" lysosomes. We detected that ~30% of all "releasable" lysosomes were liberated from the reporter cells 10 min after infection with *S. aureus* (**Figure 2**, C). Pretreatment of host cells with Vacuolin-1 or Ned-19 strongly reduced LAMP1 surface levels,

suggesting that *S. aureus* triggers lysosomal exocytosis in an NAADP-dependent manner during invasion.

To test whether lysosomal exocytosis is required for *S. aureus* internalization by host cells, we measured invasion efficiency in HuLEC (**Figure 2**, D) and HeLa cells (**Supp. Figure 2**, A) pretreated with Vacuolin-1. Invasion was strongly reduced in inhibitor-treated samples, while the survival of the bacteria was not affected by the compound (**Supp. Figure 2**, B).

Next, we triggered lysosomal exocytosis in HuLEC by addition of ionomycin prior to infection, thereby depleting the pool of "releasable" lysosomes and thus preventing lysosomal exocytosis during infection. Ionomycin pretreatment reduced invasion efficiency in a concentration-dependent manner (**Figure 2**, E). Bacterial growth and survival as well as host cell integrity were not affected at the concentrations used (1 µM, **Supp. Figure 2**, C-E).

Synaptotagmin 7 (Syt7) is known to support fusion of lysosomes with the plasma membrane in a Ca^{2+}-dependent manner (69). Accordingly, Syt7-depleted HeLa cells demonstrated lower bacterial invasion (**Figure 2**, F). As already observed for TPC1 (**Figure 1**, C), this was most pronounced early in infection. Taken together, our results support the hypothesis that lysosomal exocytosis is important for invasion of host cells by *S. aureus* particularly early during infection.

Lysosomal exocytosis results in release of ASM (6, 11), an enzyme which has previously been associated with the internalization of several bacterial and viral pathogens (8, 13, 16, 62, 63, 70) and thus, we tested if ASM activity is also required for the uptake of *S. aureus* by host cells. Therefore, we treated different cell lines prior to infection with amitriptyline, a functional inhibitor of ASM (FIASMA), or the competitive ASM inhibitor ARC39 (71) and infected host cells with *S. aureus*. While invasion in HuLEC, human umbilical vein endothelial cells (HuVEC) and HeLa was reduced by both inhibitors, invasion in bronchial epithelial $16HBE14o^{-}$ and the endothelial-epithelial hybrid cell line EA.hy926 was not or only marginally altered (**Figure 2**, G). The used inhibitor concentrations did not affect bacterial survival (**Supp. Figure 2**, F, G). Furthermore, we excluded that differences among cell lines arose from differential ASM activity or sensitivity to the inhibitors by monitoring enzymatic activity [**Supp. Figure 2**, H; (72) and **Supp. Figure 2**, I; (73)].

Next, we treated HuLEC with 10 µM ARC39 or 0.5 µM PCK310, a fast-acting ASM inhibitor. Already after 1h preincubation, PCK310 reduced invasion of *S. aureus*, whereas ARC39 required overnight treatment for a similar reduction (**Figure 2**, H). We confirmed the reduction of internalized colony forming units (CFU) by amitriptyline and PCK310 treatment with a microscopy-based approach, where we determined the number of invaded fluorescent bacteria per host cell (**Supp. Figure 2**, J).

Next, we generated two ASM-depleted HeLa cell pools (referred to as ASM K.O. 1 and 2) using CRISPR/Cas9 (74) with two distinct small guide RNAs (sgRNAs). We confirmed successful ablation of cellular ASM activity in both ASM-depleted cell lines [(73), **Supp. Figure 2**, K].

We did not detect a reduced invasion in ASM K.O. cells, when we infected in common infection medium containing 10% heat-inactivated fetal bovine serum (FBS; **Figure 2**, I).

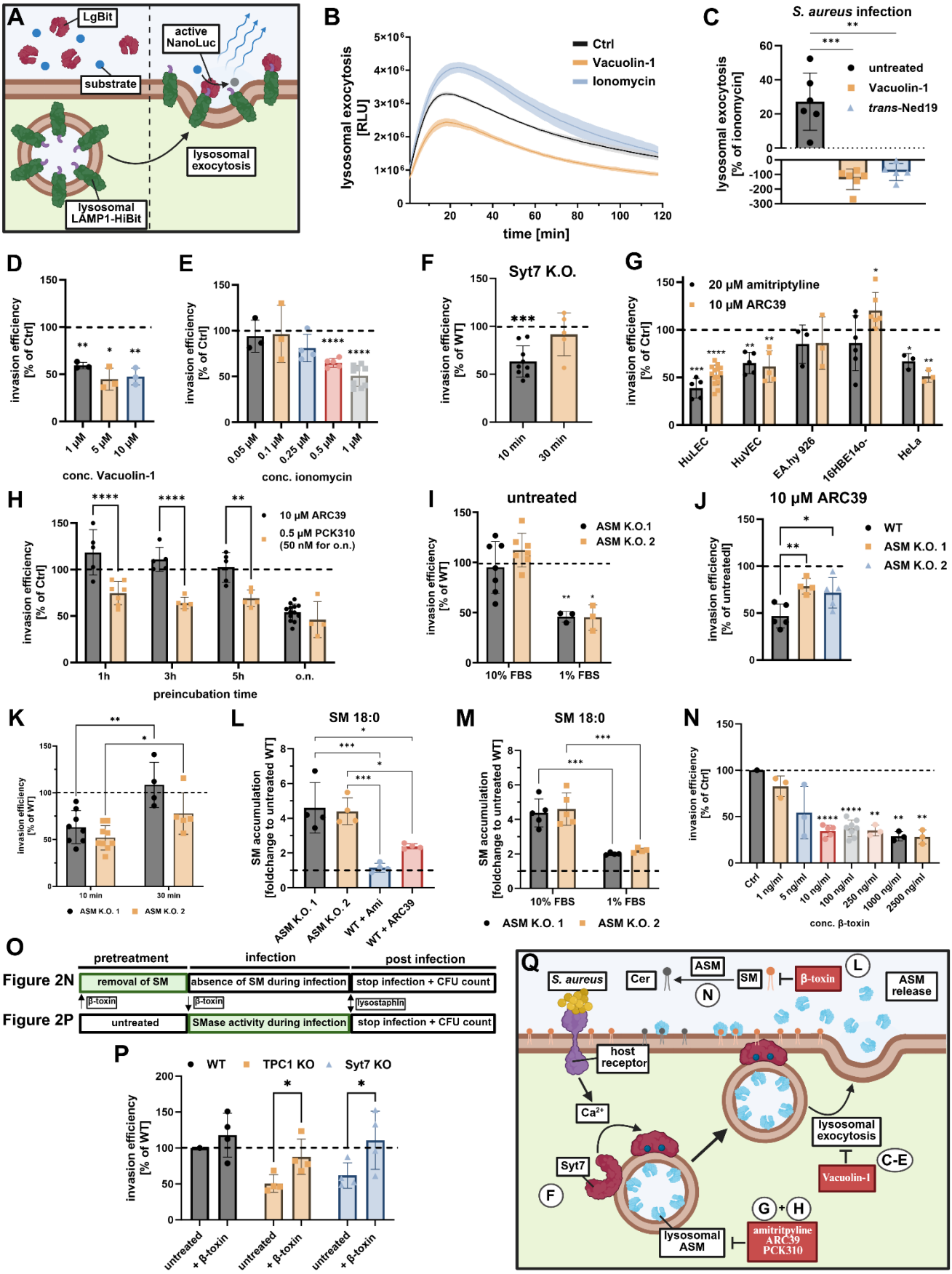

Figure 2 *S. aureus* invasion requires lysosomal exocytosis, ASM and plasma membrane sphingomyelin.
(A, B) Luminescence-based lysosomal exocytosis assay. HeLa cells expressing LAMP1-HiBit were treated with 1 µM ionomycin (immediately before the measurement) or 1 µM Vacuolin-1 (75 min before the measurement) in

presence of LgBit and NanoLuc substrate. Lysosomal exocytosis was monitored by measuring chemiluminescence in a Tecan microplate reader. n=3 **(C) *S. aureus* triggers lysosomal exocytosis during infection.** HeLa cells expressing LAMP1-HiBit were pretreated for 75 min with 1 µM Vacuolin-1 or 200 µM *trans*-Ned19. Subsequently, cells were infected with *S. aureus* JE2 (MOI10), treated with 1 µM ionomycin or left untreated and lysosomal exocytosis was determined by measuring chemiluminescence in a Tecan microplate reader 10 min p.i. Luminescence detected in infected samples was scaled to untreated controls (0 %) and ionomycin (100%) to determine the proportion of all "releasable" lysosomes liberated during infection. n=6. **(D-F) *S. aureus* invasion requires Syt7-dependent lysosomal exocytosis.** HuLEC were treated with the lysosomal exocytosis inhibitor Vacuolin-1 or the lysosomal exocytosis inducer ionomycin and invasion efficiency of *S. aureus* was determined 30 min p.i. (D, E, n≥3). Invasion efficiency of *S. aureus* JE2 was determined in HeLa Syt7 K.O. cells 10 min and 30 min p.i. (F, n≥5; data normalized to HeLa wildtype). **(G, H) *S. aureus* internalization is dependent on ASM activity in endothelial and epithelial cells.** Indicated cell lines were treated with the ASM inhibitors amitriptyline or ARC39 (G) and invasion efficiency of *S. aureus* was determined (n≥3). HuLEC were treated with PCK310 or ARC39 for the indicated periods. Subsequently, cells were infected with *S. aureus* for 30 min and invasion efficiency was determined by CFU counting (H). n≥4. **(I) *S. aureus* internalization by ASM-deficient cells is only affected when cells were cultured in medium containing low FBS concentrations.** ASM-deficient and wildtype HeLa cells were either cultured in 1% or 10% FBS prior to infection. Number of internalized bacteria was measured 10 min p.i.. Invasion efficiency was determined by normalizing the results of ASM-deficient cells to wildtype cells cultured in the corresponding FBS concentration. n≥3. **(J) Genetic ablation of ASM renders *S. aureus* invasion insensitive towards ARC39.** HeLa ASM K.O. cells were cultured in 10% FBS and treated with 10 µM ARC39 or were left untreated and the number of invaded bacteria was determined 30 min p.i.. Invasion efficiency was determined by normalization to corresponding untreated samples. n≥4 **(I) Absence of ASM has a stronger effect on *S. aureus* internalization early during infection.** ASM-deficient and wildtype HeLa cells were cultured in 1% FBS prior to infection. Invasion efficiency was determined 10 min and 30 min p.i. n≥4. **(L) Genetic ablation of ASM is accompanied by massive alteration in cellular sphingolipid profiles.** HeLa wildtype and ASM K.O. cells were treated with 20 µM amitriptyline (75 min) and 10 µM ARC39 (22h) or left untreated, as indicated**.** Whole cell sphingolipid profiles were measured by HPLC-MS/MS and foldchange of SM accumulation was determined relative to untreated wildtype cells (set to 1). Here exemplified by SM 18:0, for SM species with other acyl chain length see **Supp. Figure 3**, C. n= 4. **(M) SM accumulation is less severe when ASM-deficient cells are cultured in 1% FBS.** HeLa wildtype and ASM K.O. cells were either cultured in 1% or 10% FBS**.** Whole cell sphingolipid profiles were measured by HPLC-MS/MS and foldchange of SM accumulation in ASM K.O. cells were determined relative to untreated wildtype cells (set to 1). Here exemplified by SM 18:0, for SM species with other acyl chain length see **Supp. Figure 3**, D. **(N) *S. aureus* invasion requires SM on host cell plasma membranes.** HuLEC were treated with the bacterial SMase β-toxin for 75 min and were subsequently infected with *S. aureus* JE2 for 30 min (n≥3). **(O) Experimental design for β-toxin treatment of host cells during *S. aureus* infection.** Host cells were either pretreated with β-toxin to remove SM from the plasma membrane prior to infection (upper panel; **Figure 2, N).** Alternatively, β-toxin was added together with the bacteria to rescue the absence of ASM (lower panel, **Figure 2, P**). **(P) Presence of extracellular SMase activity restores the invasion defect in TPC1 and Syt7 K.O. cell lines.** HeLa wild type as well as TPC1 or Syt7 KO cell lines were infected with *S. aureus* JE2 in presence of 100 ng/ml of the bacterial SMase β-toxin and invasion efficiency 10 min p.i. was determined (n=4). In each experiment the numbers of intracellular *S. aureus* JE2 were determined by lysostaphin protection assay and CFU counting. Results obtained for the tested condition were normalized to the wildtype cell line or the mock-treated control. (**Q) Scheme of lysosomal exocytosis and ASM release as well as interfering agents.** Cer: ceramide, SM: sphingomyelin, ASM: acid sphingomyelinase. Statistics: one sample t-test (D-G, L), one-way ANOVA and Dunnett's multiple comparisons test (C, J). Mixed-effects model (REML) and Šídák's multiple comparisons (H). Two-way ANOVA and Tukey's multiple comparison (K). Two-way RM ANOVA and Šídák's multiple comparison (N) Bars represent means ± SD. *p≤0.05, **p≤0.01, ***p≤0.001, ****p≤0.0001.

To test if unspecific side effects of the ASM inhibitors could have contributed to reduced invasion in our previous experiments, we treated wildtype and ASM K.O.s with ARC39 and tested for *S. aureus* invasion efficiency (**Figure 2**, J). In wildtype cells, bacterial invasion again was strongly reduced after ARC39 treatment, whereas only a slight reduction was observed in the K.O.s, which may represent unspecific side effects of the inhibitor. Since the reducing effect of ARC39 on invasion is almost completely lost in ASM K.O. cells, the reduced invasion in wildtype cells upon ARC39 treatment predominantly must be caused by the inhibition of ASM.

FBS contains high levels of SM (75) as well as ASM (76), even though the enzymatic activity is strongly reduced upon heat inactivation (11).

259 To test whether FBS confounded our invasion experiments, we cultivated WT as well as ASM K.O.
260 cells in medium with reduced FBS concentration (1%) and determined the *S. aureus* invasion
261 efficiency (**Figure 2**, I). In both ASM-depleted cell lines, we detected reduced *S. aureus* invasion
262 when compared to wildtype cells only when cells were cultured in 1% FBS. Similar to our
263 observations for TPC1 and Syt7 K.O. cells, the absence of ASM had a more pronounced effect on host
264 cell entry of *S. aureus* early during infection, if cells were cultured in 1% FBS (**Figure 2**, K).

265 ASM activity in FBS could be taken up by ASM K.O. cells, thereby potentially complementing cellular
266 ASM activity and restoration of *S. aureus* invasion. However, the FBS concentration did not affect
267 cellular ASM activity of ASM K.O. cells (**Supp. Figure 2**, L).
268 Absence of ASM results in cellular accumulation of SM and usually is accompanied by the
269 neurodegenerative diseases, Niemann-Pick syndrome A and B (77). Hence, we compared the
270 sphingolipidome of inhibitor-treated wildtype and ASM K.O. cells that we either cultured in 1% or 10%
271 FBS by high-pressure liquid chromatography coupled to tandem mass spectrometry (HPLC-MS/MS).
272 Cellular SM levels were determined by ratios of SM vs. ceramide concentrations (ASM educt vs.
273 product) for lipid species with different acyl chain lengths (**Supp. Figure 3**, A and B). To assess the SM
274 accumulation upon ASM K.O. or inhibitor treatment, the fold changes of the detected SM levels
275 compared to untreated WT cells were determined (set to 1, **Supp. Figure 3**, C and D). Whereas we did
276 observe a moderate SM accumulation upon ARC39 treatment, e.g. for SM 18:0 (**Figure 2**, L) but also
277 other SM species (**Supp. Figure 3**, A and C), cells exposed to amitriptyline only showed a slight increase
278 in SM 16:0, which can be explained by the shorter preincubation time used for amitriptyline (75 min vs.
279 22h; **Supp. Figure 3**, A and C). However, if ASM K.O. cells were cultured in 10% FBS, we observed
280 markedly increased SM levels when compared to either untreated or inhibitor-treated wildtype cells [e.g.
281 for SM 18:0 (**Figure 2**, L) and other SM species (**Supp. Figure 3**, A and C)]. The relatively low increase
282 of SM levels after inhibitor treatment likely arises from short inhibitor pulses (in the range of minutes
283 or hours), whereas SM in ASM K.O. cell lines accumulates over the entire culture period (days or weeks
284 since gene ablation). Strikingly, ASM K.O. cells accumulated markedly less SM 18:0 (**Figure 2**, M),
285 SM 16:0 and SM 20:0 (**Supp. Figure 3**, D), when cultured in 1% FBS, suggesting that FBS is an
286 important source of SM in absence of ASM.
287 In summary, we detected moderate SM accumulation in conditions (ASM inhibitor treatment or ASM
288 K.O.s cultured in 1% FBS) where we also detected reduced *S. aureus* invasion and a strong SM
289 accumulation (ASM K.O. cultured in 10% FBS) when the number of internalized bacteria was not
290 affected when compared to untreated wildtype cells.
291 We hypothesize that strong cellular SM accumulation generally increases ASM-independent host cell
292 invasion of *S. aureus*, while the ASM-dependent uptake pathway is absent. This is supported by the high
293 residual internalization of *S. aureus* by ASM K.O. cells cultured in 10% FBS upon ARC39 treatment.
294 Previously, it was shown that *S. aureus* host cell entry is limited by caveolin-1, a protein associated with
295 lipid microdomains (78, 79). Absence of ASM was demonstrated to interfere with caveolin-1-
296 associateded endocytosis (80, 81) and thus, the increased invasion in ASM K.O. cells may be caused by
297 dysfunctional caveolin-1.
298 Taken together, our results show that ASM is involved in *S. aureus* invasion of host cells in a cell-type
299 specific manner.
300 Release of ASM by host cells results in cleavage of SM on the host cell surface, a process that previously
301 was suggested to facilitate cell entry of human pathogens (7, 8, 13-17). To test whether *S. aureus*
302 invasion requires SMase activity on the host cell surface, we removed SM, the substrate of ASM, from
303 plasma membranes of HuLEC (**Figure 2**, N) and HeLa (**Supp. Figure 2**, M) by pretreatment with the
304 bacterial SMase β-toxin (see **Figure 2**, O). We confirmed β-toxin-dependent SM conversion in living
305 cells by detecting the ceramide metabolites of fluorescent SM analogs [**Supp. Figure 2**, N; (82)].
306 Plasma membrane pretreatment with bacterial SMase reduced *S. aureus* invasion efficiency in a
307 concentration-dependent manner in both cell lines. 10 ng/ml β-toxin were sufficient to decrease invasion

308 to ~30% of that measured in untreated control cells. Interestingly, a 250-fold higher concentration did
309 not lead to further reduction, suggesting that 10 ng/ml β-toxin were sufficient to quantitatively convert
310 SM to ceramide at the cell surface. In line with our previous experiments, this suggests that multiple *S.*
311 *aureus* invasion pathways exist within the same host cell population, of which at least one requires SM
312 and its enzymatic breakdown on the plasma membrane.
313 Since we detected enhanced Ned19-sensitive lysosomal exocytosis during *S. aureus* infection (**Figure**
314 **2**, C), we hypothesized that absence of TPC1 or Syt7 should impair lysosomal exocytosis and thereby
315 release of ASM. Therefore, we infected wildtype as well as TPC1 or Syt7 K.O. cells with *S. aureus* in
316 presence (but without pretreatment, see **Figure 2**, O) of 100 ng/ml β-toxin and determined the number
317 of intracellular bacteria after 10 min (**Figure 2***,* P). The addition of β-toxin to the culture medium
318 completely rescued the invasion defect of the K.O. cells. This indicates that reduced bacterial
319 internalization in absence of TPC1 and Syt7 results from a lack in ASM delivery to the cell surface by
320 Ca^{2+}-dependent lysosomal exocytosis and that absence of ASM from the host cell surface, can be
321 compensated by exogenous addition of the bacterial SMase β-toxin.
322 We want to emphasize the difference in experimental application of β-toxin (**Figure 2**, O) where we i)
323 pretreat host cells with the bSMase to remove SM from the plasma membrane (**Figure 2**, N and **Supp.**
324 **Figure 2**, M) and ii) rescue the absence of exocytosed ASM from the host cell surface by exogenous
325 addition of β-toxin during the infection (**Figure 2***,* P). In the former case, pretreatment leads to removal
326 of SM from the plasma membrane thus preventing SM conversion by ASM during infection and
327 resulting in reduced invasion. The latter leads to SM conversion by the bacterial SMase during infection
328 thereby increasing invasion.
329 In summary, our data suggest the existence of a *S. aureus* invasion pathway that depends on the
330 metabolic breakdown of SM by ASM on the host cell surface (**Figure 2**, Q).
331
332 ***ASM- and Ca^{2+}-mediated invasion is rapid***
333 To study the role of SM in *S. aureus* uptake kinetics, we incubated HuLEC with fluorescent sphingolipid
334 analogs and recorded *S. aureus* infection by time lapse imaging [**Figure 3**, A; **Supp. Video 1**; **Supp.**
335 **Figure 4**; **Supp. Video 2**; (73)]. We observed that the bacteria were rapidly engulfed by SM-containing
336 membrane compartments. While association of bacteria with BODIPY-FL-C12-SM increased over time
337 during the first 30 min of infection, this was not observed for BODIPY-FL-C12-Ceramide, suggesting
338 that *S. aureus* invasion specifically relies on interaction with SM in host cell plasma membranes (**Figure**
339 **3**, B).
340 Next, we determined the invasion efficiency of *S. aureus* in a time-dependent manner and blocked
341 invasion by either ASM inhibitors, ionomycin, BAPTA-AM or β-toxin pretreatment. We found a time-
342 dependent increase in intracellular bacteria, whereby all treatment conditions reduced bacterial invasion
343 at every time point with the untreated control at 30 min set to 100% (**Figure 3**, C). We next normalized
344 the data to the untreated control of the corresponding time point. Except for the β-toxin treatment, the
345 effect of all other treatments was most pronounced early (5-10 min) after infection (**Figure 3**, D). For
346 instance, ionomycin treatment massively reduced *S. aureus* invasion to ~20% of untreated controls when
347 we infected for 10 min. We concluded that in untreated controls 80% of the bacteria entered host cells
348 via the pathway that depends on lysosomal exocytosis, Ca^{2+} and ASM, which is blocked by ionomycin
349 treatment. Consequently, bacteria that were able to invade host cells in ionomycin-treated samples (the
350 residual ~20%) must have employed other pathways. By contrast, in samples infected for 30 min a
351 higher proportion of bacteria was able to enter host cells despite ionomycin treatment (~50% compared
352 to untreated controls). This suggests that only 50% of all invaded bacteria were internalized in an ASM-
353 and Ca^{2+}-dependent fashion upon the longer infection pulse. Together with the observed invasion defects
354 in host cells with gene deletions in TPC1 (**Figure 1**, C), Syt7 (**Figure 2**, F) and ASM (**Figure 2**, K),
355 which we exclusively detected during short infection times, our data suggest that early during infection
356 bacteria enter host cells predominantly in an ASM- and Ca^{2+}-dependent manner. Thus, we concluded

that the internalization pathway that depends on lysosomal exocytosis, ASM and Ca^{2+} is rapid when compared to other host cell entry pathways.

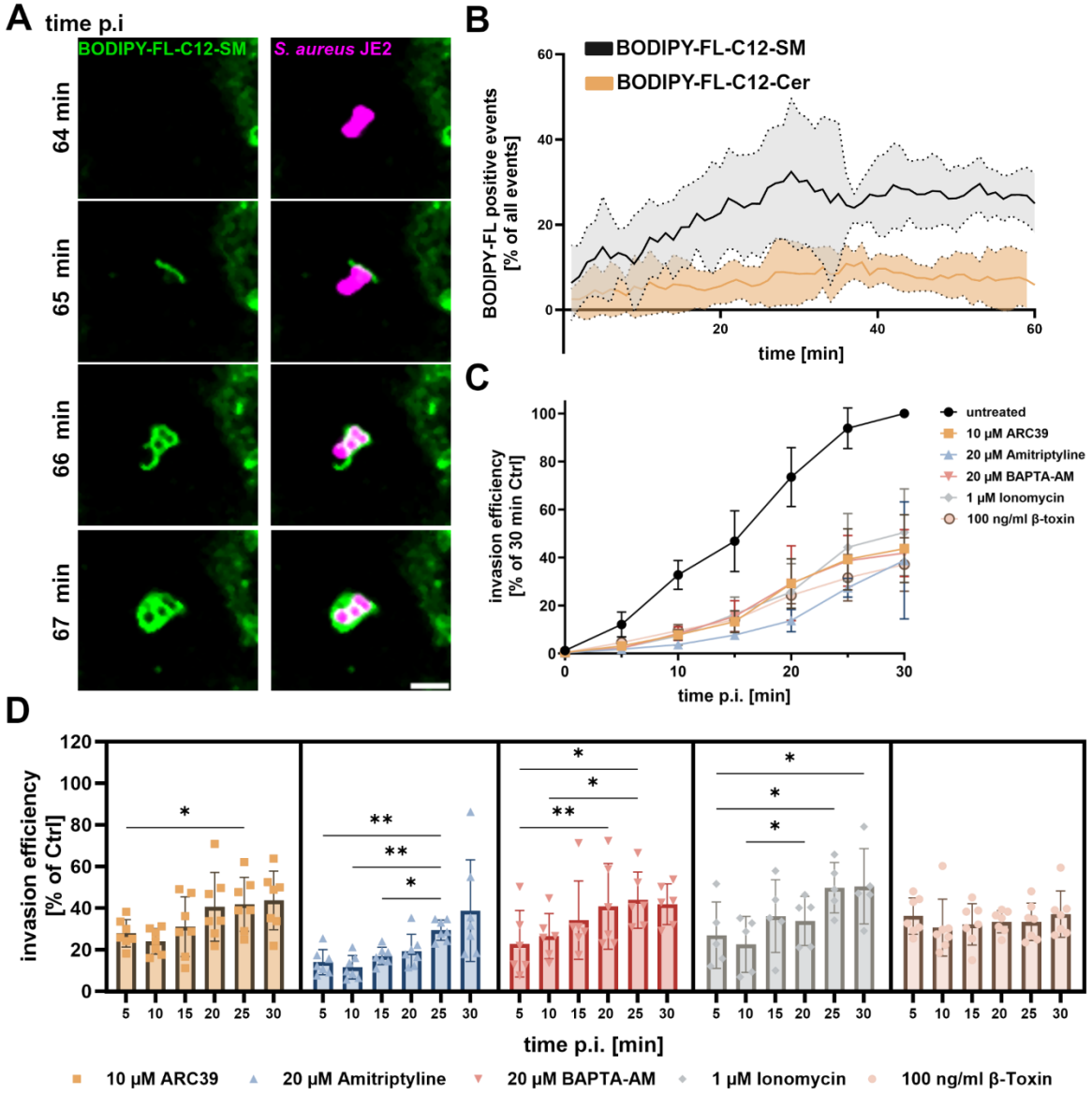

Figure 3 ASM- and Ca^{2+}-dependent uptake is rapid and predominantly mediates invasion early in infection. (A, B) *S. aureus* associates with SM early during invasion. HuLEC were pretreated with BODIPY-FL-C12-SM or BODIPY-FL-C12-ceramide and infected with red-fluorescent *S. aureus*. Scale bar: 5 µm. Infection was monitored by live cell imaging and the proportion of bacteria that associated with the lipid analogs was quantified in each individual frame (SM: n=5, Cer: n=3). **(C, D) ASM and Ca^{2+}-dependent invasion is rapid.** HuLEC were treated with ARC39, amitriptyline, BAPTA-AM, ionomycin, or the bacterial SMase β-toxin. Then, cells were infected with *S. aureus* and the number of invaded bacteria was determined after different time periods. The results were either normalized to the 30 min time point of untreated controls (C) or to the corresponding time points of the untreated controls (D). (n ≥5). Statistics: Mixed effect analysis and Tukey's multiple comparison. Graphs represent means ± SD. *p≤0.05, **p≤0.01, ***p≤0.001, ****p≤0.0001.

The mode of S. aureus invasion affects infection outcome

Next, we tested whether the pathway used for host cell entry also affects the intracellular fate of *S. aureus*. After invasion, the bacteria reside within Rab5-positive early and subsequently, in Rab7-positive late phagoendosomes (39). To trace phagosome maturation, we generated a HeLa cell line stably expressing mCherry-Rab5 as well as YFP-Rab7 and infected with *S. aureus*. We observed that the

376 bacteria transiently associate with Rab5 for a few minutes, before they become positive for Rab7
377 (**Supp. Video 3**).
378 We next blocked the ASM-dependent invasion pathway by amitriptyline treatment and infected with *S.*
379 *aureus* for different time periods. We determined the proportion of bacteria that was associated with
380 Rab5 and/or Rab7 (**Figure 4**, A; see **Supp. Figure 5** for bacteria proportion that associates with Rab7).
381 While ASM inhibition only marginally affected *S. aureus* association with Rab5-positive phagosomes,
382 the proportion of bacteria residing in Rab7-positive vesicles was significantly reduced when compared
383 to the untreated control. This observation was restricted to shorter infection pulses (5-45 min) and was
384 not observed for long infection periods (60 min).
385 We also observed a reduced proportion of bacteria associated with Rab7-positive membranes after
386 treatment with PCK310 or bacterial SMase (**Supp. Figure 5**, B, C). Forty-five minutes p.i., about half
387 of the bacteria were localized to Rab7-positive vesicles in untreated cells, whereas only ~40% associated
388 with Rab7 upon amitriptyline, PCK310 or β-toxin treatment (**Supp. Figure 5**, C). However, this was
389 not caused by translocation of *S. aureus* to the host cytosol, which was excluded by expressing the
390 fluorescence reporter RFP-CWT (42) in the YFP-Rab7 cell line. Accordingly, RFP-CWT-labelled
391 bacteria in the host cytosol were excluded from the data set [**Supp. Figure 5**, B-D,, (42)]. Hence, ASM-
392 dependently generated phagoendosomes possess different maturation dynamics when compared to
393 phagosomes formed in an ASM-independent fashion.
394 Next, we measured phagosomal escape while simultaneously detecting SM content of disrupted
395 phagosomal membranes. Therefore, we used a HeLa reporter cell line that cytosolically expresses the
396 phagosomal escape reporter RFP-CWT (42) as well as the SM reporter Lysenin^{W20A}-YFP (83),
397 respectively (**Figure 4**, B). To validate the reporter system, we removed SM from the plasma membrane
398 by β-toxin treatment prior to infection and monitored phagosomal escape by live cell imaging (**Supp.**
399 **Figure 6**, **Supp. Video *4***). Bacterial translocation into the host cytosol is, again, indicated by recruitment
400 of RFP-CWT. In untreated cells, phagosomal escape was accompanied by recruitment of Lysenin^{W20A}-
401 YFP to vesicular membranes, suggesting that SM located at the luminal leaflet of phagosomes was
402 exposed to the cytosol. By contrast, Lysenin^{W20A}-YFP was not recruited to escape events in β-toxin-
403 treated cells, indicating that the SMase had removed SM from the membranes.
404 Next, we tested whether internalization of the bacteria via the ASM-dependent pathway would affect
405 phagosomal escape of *S. aureus*. We first confirmed that invasion of *S. aureus* is sensitive to ASM
406 inhibitors and β-toxin treatment, despite reporter gene expression in the cell line (**Supp. Figure 5**, E).
407 Then reporter cells either were left untreated or were pre-exposed to ASM inhibitors and were infected
408 with *S. aureus* strain JE2. In addition, *S. aureus* Cowan I, a non-cytotoxic strain known to have low
409 escape rates, was used for infection. The proportion of bacteria that escaped from the phagosome
410 (**Figure 4**, C, D) as well as the proportion of escape events, which were additionally positive for
411 cytosolic SM (**Supp. Figure 5**, F) were determined 1.5 h and 3 h p.i. (see also **Supp. Figure 7**, A-D).
412 Whereas no differences for Lysenin-positive escape events were detected (**Supp. Figure 5**, F), a higher
413 proportion of bacteria escaped from phagosomes on abrogation of ASM activity regardless of the
414 inhibitor used (**Figure 4**, C, D). A similar increase was observed when we blocked lysosomal exocytosis
415 by Vacuolin-1 ((**Figure 4**, E), suggesting that the lack of ASM delivery to the host cell surface during
416 bacterial invasion affects phagosomal escape.

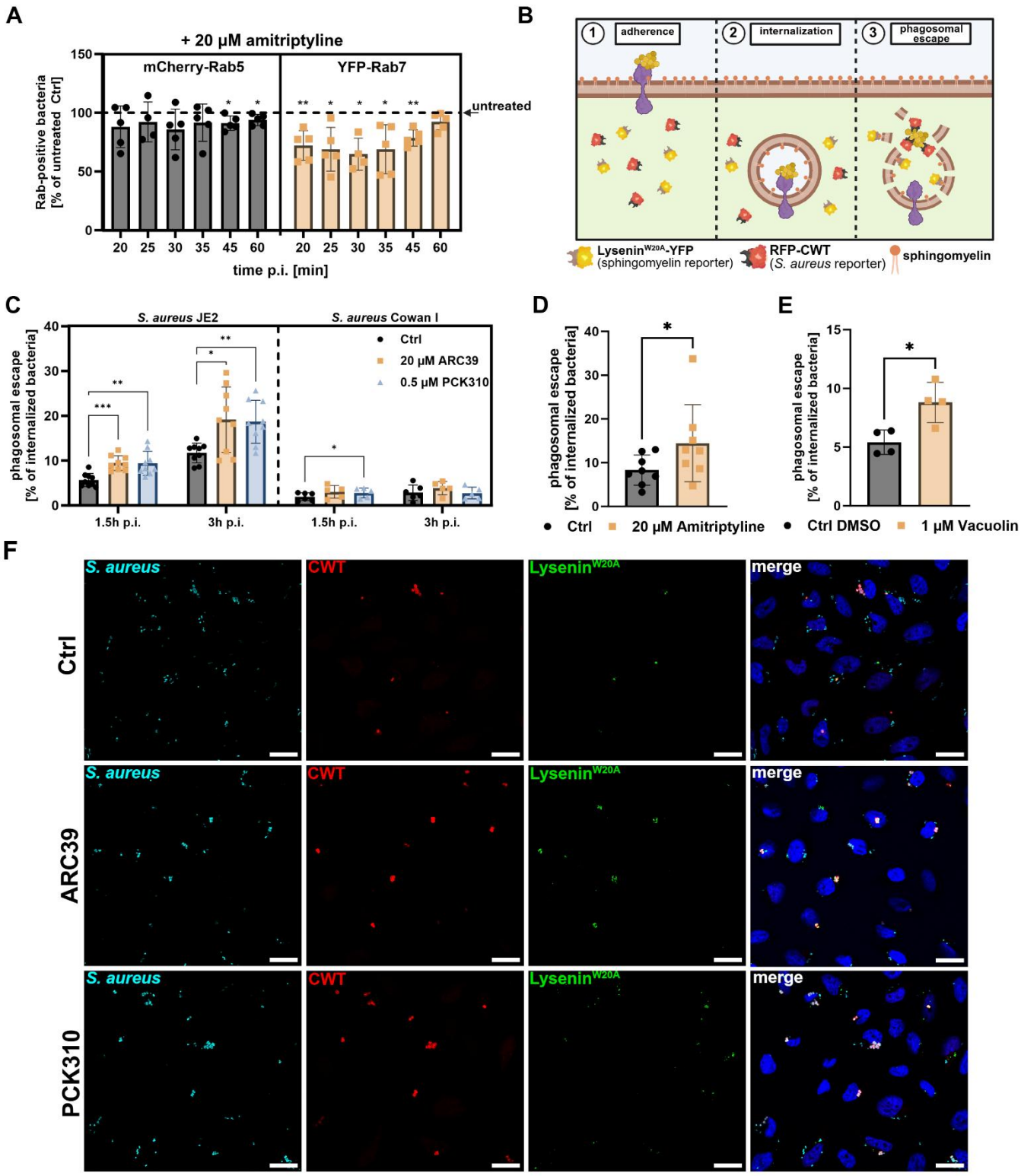

Figure 4 Blocking ASM-dependent invasion affects phagosomal maturation and escape during *S. aureus* infection

(A) Inhibition of ASM delays formation of Rab7-positive phagosomes. HeLa cells expressing mCherry-Rab5 and YFP-Rab7 were either treated with amitriptyline or left untreated. Then, cells were infected with *S. aureus* JE2 for indicated periods. Extracellular bacteria were removed and percentage of intracellular bacteria which associated with Rab5 or Rab7 was determined by CLSM. Results obtained for amitriptyline-treated samples were normalized to untreated controls (n=5). **(B) Detection of phagosomal SM and phagosomal escape by a reporter cell line expressing Lysenin^{W20A} -YFP and RFP-CWT.** After internalization, *S. aureus* resides in a phagosome preventing the recruitment of RFP-CWT to *S. aureus* cell wall and Lysenin^{W20A}-YFP to luminal SM, respectively. When the bacteria lyse the phagosomal membrane, luminal SM gets exposed to the cytosol and attracts

Lysenin^{W20A} -YFP, while RFP-CWT is recruited to the staphylococcal surface. (**C-F) Blocking ASM-dependent internalization affects phagosomal escape.** RFP-CWT and Lysenin^{W20A} -YFP expressing HeLa were treated with PCK310,ARC39 (C, F), amitriptyline (D) or Vacuolin-1 (E) and infected with *S. aureus* strains JE2 or Cowan I. By CLSM, proportions of bacteria that recruited RFP-CWT (phagosomal escape) were determined 3h p.i. if not indicated otherwise (n≥3). **Statistics:** one sample t-test (A), Mixed effects analysis (REML) and Tukey's multiple comparison (C,), paired Student´s t-test (D, E) Graphs represent means ± SD. *p≤0.05, **p≤0.01, ***p≤0.001, ****p≤0.0001.

Since blocking of ASM-dependent uptake reduced invasion efficiency yet increased phagosomal escape rates, we hypothesized that the presence of SM on the plasma membrane affects downstream events during *S. aureus* infection. To address this, we pretreated host cells with the bacterial SMase β-toxin to block SM-dependent invasion (**Figure 5**, A; 2a, 2b) and either infected the cells in presence (**Figure 5, A;** 3a) or after removal of the toxin (3b). β-toxin pretreatment, resulted in enhanced phagosomal escape rates of *S. aureus* JE2, independent of the presence of β-toxin during infection (**Figure 5**, B; 4a, 4b). This was not observed for infections with the Cowan I strain, indicating that removal of SM by β-toxin did not affect general phagosomal membrane stability (**Supp. Figure 5**, G). Moreover, β-toxin treatment strongly reduced recruitment of Lysenin^{W20A}, demonstrating effective removal of SM from membranes by β-toxin (**Figure 5**, C and **Supp. Figure 7**, E-J).

To investigate if removal of SM was important at the cell surface or within the phagosome, we infected the cells with transgenic *S. aureus* JE2 strain either collinearly overexpressing β-toxin and cyan-fluorescent reporter Cerulean or solely expressing Cerulean. We did not observe increased phagosomal escape upon overexpression of β-toxin (**Figure 5**, B; 4c), although Lysenin recruitment to phagosomal membranes was reduced to levels of β-toxin-pretreated samples (**Figure 5**, C). Moreover, we did not detect substantial differences in escape rates of *S. aureus* 6850, a strain naturally producing β-toxin (**Supp. Figure 5**, H), and its isogenic β-toxin mutant. Again, escape of *S. aureus* 6850 was enhanced upon pretreatment with β-toxin (**Supp. Figure 5**, I) accompanied by absence of SM from phagosomal membranes (**Supp. Figure 5**, J).

Phagosomal escape of *S. aureus* thus is independent of SM levels within the infected phagosomes but rather reflects the presence of SM and ASM at the plasma membrane during host cell entry.

We previously showed that *S. aureus* predominantly enters host cells via the rapid ASM- and Ca^{2+}-dependent pathway early upon host cell contact (**Figure 1**, C; **Figure 2**, F; **Figure 3**, D), while other pathways are likely employed later during infection. Consequently, the proportion of pathways (ASM-dependent vs. ASM-independent) that is used for host cell entry relies on the infection time. To demonstrate that phagosomal escape is dependent on the pathway of cell entry, we infected reporter cells with *S. aureus* for either a 10 min ("early invaders") or a 30 min infection pulse (representing "early and late invaders") and at 3h p.i. we determined phagosomal escape rates (**Figure 5**, D) as well as the number of invaded bacteria (**Supp. Figure 5**, K). Independent of the multiplicity of infection (MOI) used, bacteria taken up within the first 10 min demonstrated significantly lower escape rates when compared to bacteria that were cocultured with host cells for 30 min.

This was corroborated by HeLa YFP-CWT infected with *S. aureus* expressing a fluorescent protein (e.g. mRFP) for 30 min ("early and late invaders"). After 20 min, we initiated a second infection pulse for 10 min ("early invaders") with a *S. aureus* strain expressing another fluorescence protein (e.g. Cerulean) and determined phagosomal escape rates of both bacterial recombinants (**Figure 5**, E). Again, early invaders demonstrated lower escape rates when compared to the 30 min control. This was independent of the fluorescent marker expressed by the strain that was used for each infection pulse.

Taken together, we observed higher escape rates 3h p.i., whenever we blocked the rapid ASM-dependent invasion pathways. Consistently, escape rates of bacteria predominantly internalized via the ASM-dependent route ("early invaders") were decreased (**Figure 5**, F). Hence, we concluded that the pathway of host cell entry directly affects phagosomal escape.

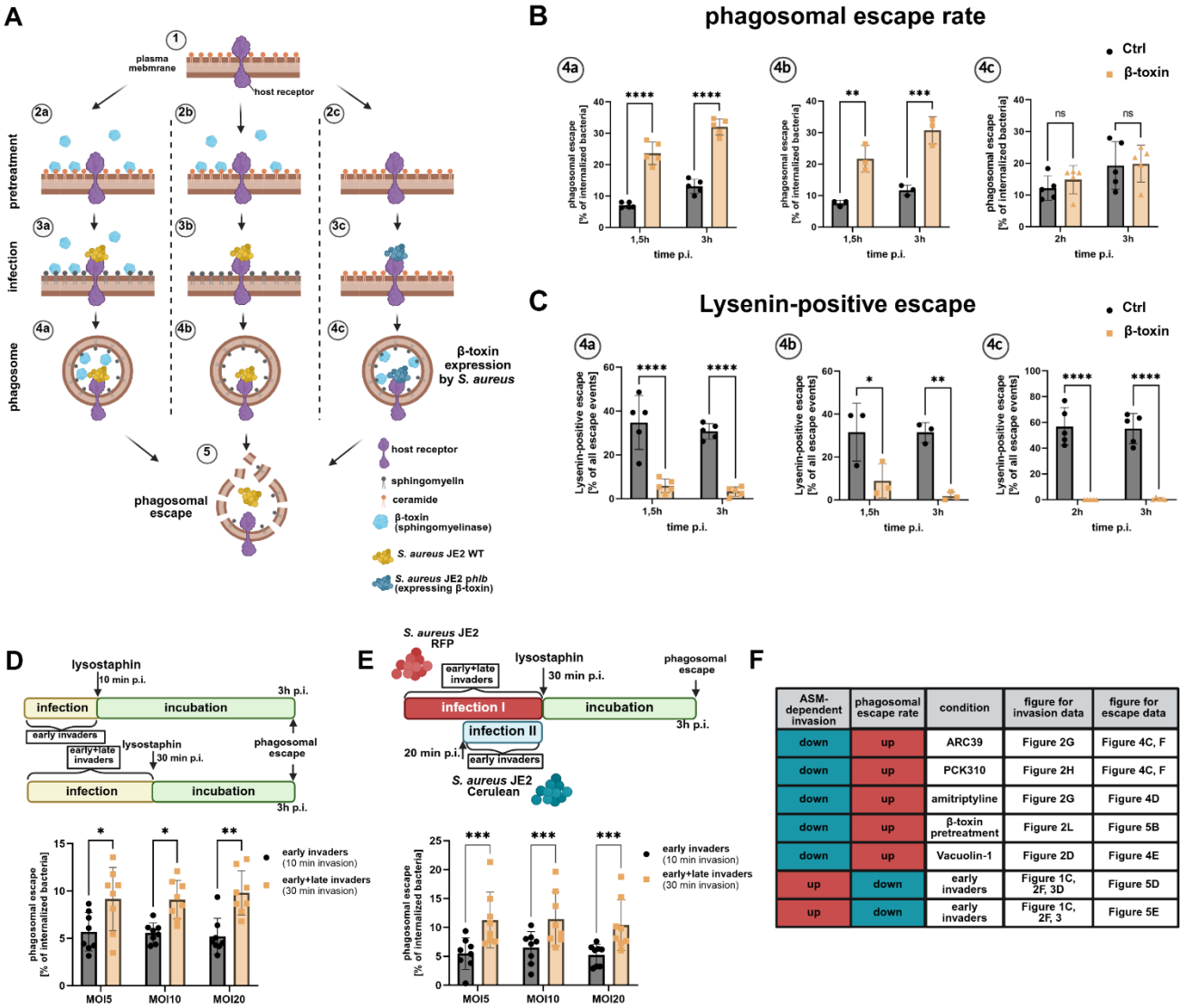

ASM-dependent invasion	phagosomal escape rate	condition	figure for invasion data	figure for escape data
down	up	ARC39	Figure 2G	Figure 4C, F
down	up	PCK310	Figure 2H	Figure 4C, F
down	up	amitriptyline	Figure 2G	Figure 4D
down	up	β-toxin pretreatment	Figure 2L	Figure 5B
down	up	Vacuolin-1	Figure 2D	Figure 4E
up	down	early invaders	Figure 1C, 2F, 3D	Figure 5D
up	down	early invaders	Figure 1C, 2F, 3	Figure 5E

Figure 5 The intracellular fate of *S. aureus* is determined by host cell entry

(A-C) Phagosomal escape depends on presence of plasma membrane SM during invasion, but not presence of SM within phagosomal membranes HeLa RFP-CWT Lysenin^{W20A} -YFP were pretreated with β-toxin to remove surface SM (2a, 2b) or left untreated (2c). Then, cells were infected with *S. aureus* JE2 in presence (3a) or absence (3b) of β-toxin. Untreated samples (3c) were infected with *S. aureus* JE2 harboring a plasmid either encoding β-toxin and the fluorescence protein Cerulean (pCer+*hlb*) or solely Cerulean (pCer). Proportion of bacteria that recruited RFP-CWT (phagosomal escape, B) and the percentage of phagosomal escape events that additionally were positive for Lysenin^{W20A}-YFP (C) were determined at indicated time points p.i. (n=5). **(D, E) Early ASM-dependent invaders possess lower escape rates than late invaders.** HeLa cells expressing RFP-CWT were infected with indicated MOIs of *S. aureus* JE2 either for 10 min (early invaders) or 30 min (early+late invaders). Phagosomal escape rates were determined 3h p.i. (D). HeLa reporter cells expressing YFP-CWT were infected with an MOI=5 of *S. aureus* JE2 expressing a fluorescent protein (e.g. RFP) for 30 min (early+late invaders). After 20 min, the same samples were infected with *S. aureus* JE2 expressing another fluorophore (e.g. Cerulean) for 10 min (early invaders) and phagosomal escape was determined 3 h p.i. (E). **(F) Summary of experiments analyzing the influence of invasion pathway on phagosomal escape.** The measured effects of different conditions on rapid ASM-dependent invasion and accompanied alterations in phagosomal escape rates are summarized. red = increased, blue=decreased. **Statistics:** Two-way ANOVA and Šídák's multiple comparisons test (B-E). Graphs represent means ± SD. *p≤0.05, **p≤0.01, ***p≤0.001, ****p≤0.0001.

We next monitored phagosomal escape over 10 h in cells pretreated with ASM inhibitors (**Figure 6**, A, see **Supp. Figure 8**, for absolute bacteria numbers of individual replicates). ASM inhibition enhanced escape rates 3 h p.i. when compared to untreated controls. In contrast, 6 h p.i. escape rates were found decreased upon ASM inhibition.

Taken together, the efficiency of phagosomal escape of *S. aureus* is directly affected by the mode of cell entry, whereby the rapid SM/ASM-dependent pathway results in delayed phagosomal escape, while bacteria that entered host cells ASM-independently escape earlier during infection.

Since translocation to the host cytosol is a prerequisite for *S. aureus* replication in non-professional phagocytes, we recorded intracellular growth of *S. aureus.* In untreated controls replication started about 5 h p.i., and thus shortly after phagosomal escape (3-4 h p.i., **Figure 6**, B). By contrast, we did not observe significant bacterial replication in cells treated with ASM inhibitors (**Figure 6**, B).

We next treated HuLEC with β-toxin, stained the cells with BODIPY-FL-C12-SM and infected the cells with fluorescent *S. aureus*. Live cell imaging demonstrated that most untreated host cells died after 11 h p.i., whereas β-toxin-treated samples showed higher survival rates (**Figure 6**, C). This was also observed by cell death assays measuring i) membrane integrity (7-AAD staining, **Figure 6**, D), ii) apoptosis (Annexin V staining, **Figure 6**, E), iii) number of host cells that remained attached to the substratum (**Supp. Figure 9**, A) and iv) host cell lysis by LDH release (**Supp. Figure 9**, B) at 21 h p.i..

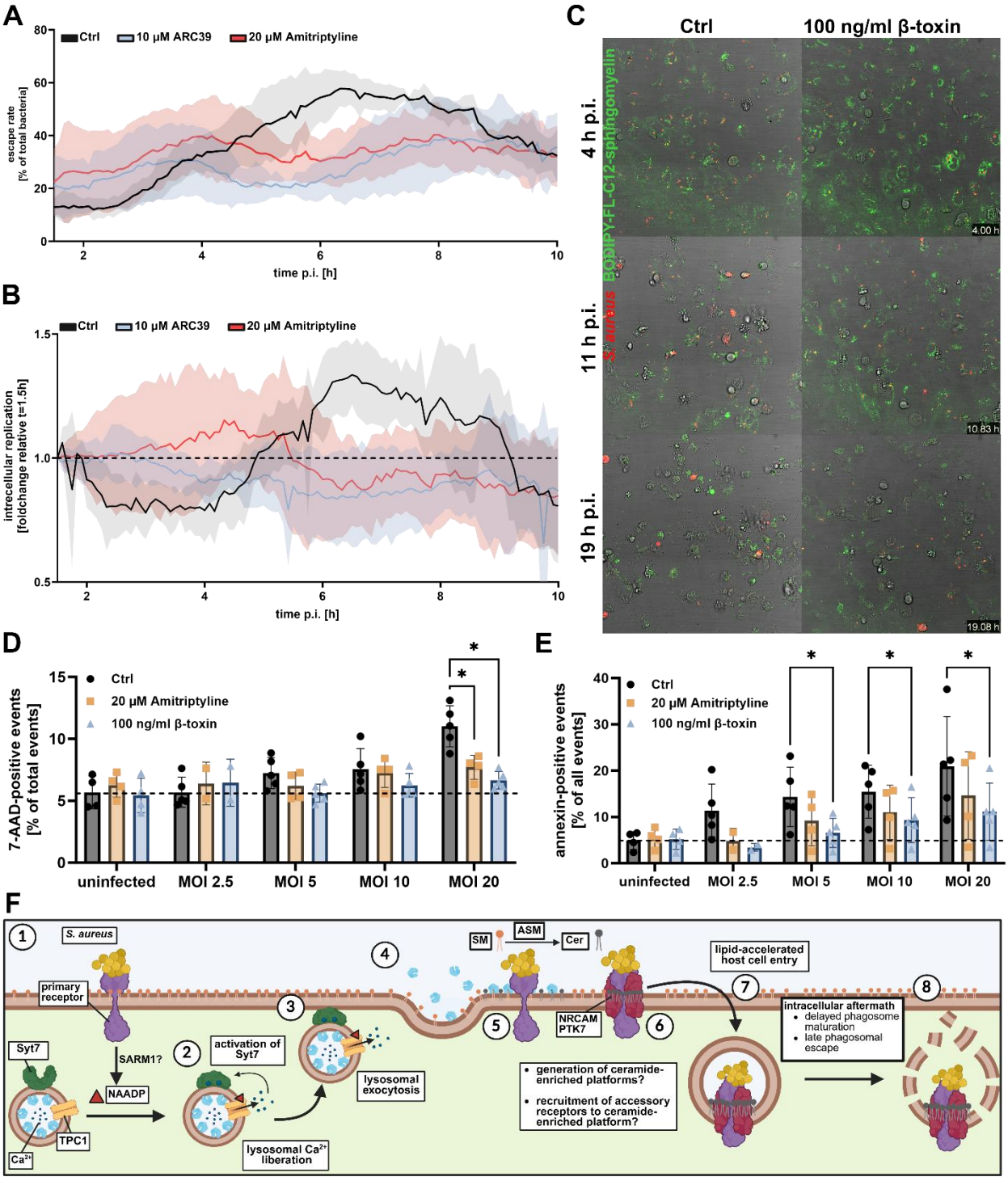

Figure 6 Blocking ASM-dependent internalization affects intracellular replication and host cell survival. **(A, B)** HeLa cells expressing RFP-CWT and Lysenin^{W20A}-YFP were treated with amitriptyline or ARC39 or were left untreated (Ctrl). The cells were subsequently infected with *S. aureus* and infection was monitored for 10 h by CLSM. Proportion of escaped bacteria (A) or the intracellular replication (B) was determined (n= 5). **(C)** HuLEC were stained with BODIPY-FL-C12-SM (green), and were either pretreated with 100 ng/ml of β-toxin or were left untreated. Then, cells were infected with *S. aureus* (red) and infection was monitored by CLSM for 19 h. **(D, E)** HuLEC were treated with amitriptyline or β-toxin and subsequently infected with *S. aureus*. After 21 h, plasma membrane integrity was measured by 7-AAD staining (D), and proportion of apoptotic cells was determined by annexin V staining (E) (n=5). See also **Supp. Figure 9**. (F) Model: *S. aureus* interacts with an unknown primary receptor (1) that triggers production of NAADP, which in turn activates TPC1 to mediate lysosomal Ca^{2+} release and activation of Syt7 (2). Syt7-dependent lysosomal exocytosis (3) leads to release of

ASM (4) and production of Cer on the plasma membrane (5) thereby presumably resulting in the recruitment of co-receptors [6,(84)] and rapid internalization of *S. aureus* by host cells (7). Bacteria, which enter the host cells via the rapid pathway, experience a different intracellular fate than bacteria that employed other pathways. **Statistics:** Mixed effects analysis (REML) and Tukey‘s multiple comparison test. Graphs represent mean ± SD. *$p \leq 0.05$.

Discussion

ASM has been previously reported to be implicated in the invasion of several viral, bacterial, and eukaryotic pathogens (7, 8, 13-17). However, the dynamics of ASM-mediated host cell entry, the underlying receptors as well as effects on post-invasion events are only poorly understood.

We here show that ASM is involved in the uptake of *S. aureus* by certain human cells within minutes after the pathogen contacts the host cell and this pathway is concurrent with ASM-independent uptake pathways. We demonstrate that the infection outcome of bacteria that enter the host cells via this rapid pathway is distinct from other entry mechanisms.

We observed a reduction of bacterial invasiveness upon treatment with different ASM inhibitors (**Figure 2**, G) or removal of the enzyme substrate SM from the plasma membrane (**Figure 2**, N) suggesting that ASM activity on the host cell surface is crucial for pathogen internalization. Since it remains elusive to which extent ASM processes SM on the plasma membrane during *S. aureus* invasion, one may speculate that ASM could also have functions other than SM metabolization during host cell entry of the pathogen. However, we did not detect a direct interaction between *S. aureus* and ASM in an *S. aureus*-host interactome screen (84).

Surprisingly, the uptake of *S. aureus* by ASM-deficient cells was only reduced relative to the wild type when cells were cultured in 1% but not in 10% FBS, a concentration commonly used in culture media (**Figure 2**, I). In ASM K.O.s cultured in 10% FBS, *S. aureus* invasion was only slightly affected by the ASM inhibitor ARC39, while ARC39-treated wildtype cells showed a stronger reduction (**Figure 2**, J). We concluded that reduced invasion in wildtype cells upon ARC39 treatment is mostly due to inhibition of ASM and consistently, the effect of ARC39 is strongly attenuated in ASM K.O.s. Hence, we postulate that other ASM-independent host cell pathways are upregulated in ASM-deficient cells cultured in 10% FBS, which might be caused by the strongly altered sphingolipid profile of these cells (**Figure 2**, L, M; **Supp. Figure 3**). Consistently, culturing ASM-deficient cells in 1% FBS resulted in less severe SM accumulation (**Figure 2**, M; **Supp. Figure 3**, B and D) and a reduced *S. aureus* invasion compared to wildtype cells (**Figure 2**, I).

For instance, *S. aureus* internalization by host cells is strongly restricted by caveolin-1, a protein associated with lipid membrane domains (78, 79). Accordingly, alterations in membrane composition might affect distribution of caveolin-1 on the plasma membrane, thereby fostering uptake of *S. aureus*. In consistency, previous studies reported dysfunction of caveolin-1-dependent endocytic processes in ASM-deficient cells (80, 81).

Release of ASM is caused by lysosomal exocytosis (6). Conventional methods for detection of lysosomal exocytosis often depend on the usage of anti-LAMP1 antibodies that are added to the cell culture medium for monitoring LAMP1 exposure on the plasma membrane (66). However, most antibodies are non-specifically bound by staphylococcal protein A (85) and hence, these protocols are not compatible with *S. aureus* infection studies. Therefore, we developed a novel approach to measure lysosomal exocytosis via a split luciferase-based assay that demonstrated lysosomal exocytosis during *S. aureus* infection (**Figure 2**, A-C). Consequently, depleting host cells from lysosomes that can undergo Ca^{2+}-dependent exocytosis by ionomycin pretreatment, reduced invasion, even though ionomycin can influence general host cells Ca^{2+} homeostasis (86). Additionally, the lysosomal exocytosis inhibitor Vacuolin-1 resulted in drastically reduced internalization of bacteria (**Figure 2**, D), although the substance is known for side effects such as inhibition of PIKfyve thereby affecting the endo-lysosomal compartment (87). However, we confirmed the role of lysosomal exocytosis for *S. aureus* invasion of host cells by genetic ablation of Syt7, a key protein in lysosomal exocytosis (69).) It remains elusive,

587 which other factors are involved in delivery of lysosomes to and fusion of lysosomes with the plasma
588 membrane. Next to Syt7, there might be other proteins such as Synaptotagmin 1 with overlapping
589 function that could compensate for the absence of Syt7 (88).
590 Elevation of cytosolic Ca^{2+} levels lead to recruitment of lysosomes to the cell surface (67). Whereas
591 most studies implicated Ca^{2+} influx from the extracellular milieu (7, 16), we here demonstrate that *S.*
592 *aureus* mainly triggers lysosomal Ca^{2+} mobilization as was shown by treatment with the inhibitor *trans*-
593 Ned19 as well as a genetic K.O. of the endo-lysosomal Ca^{2+} channel TPC1 (**Figure 1**, B and E; **Supp.**
594 **Figure 1**, C). Since fluorescent calcium reporters allow to monitor this process microscopically (89,
595 90), future experiments may visualize this process in more detail and contribute to our understanding of
596 the underlying signaling mechanisms.
597 There are two TPCs (TPC1 and TPC2) that mediate lysosomal Ca^{2+} liberation (91), which have
598 previously been associated with regulation of phagocytic processes (90) and host cell entry of several
599 viruses such as Ebola virus (92), Middle East respiratory syndrome coronavirus [MERS-CoV, (93)] or
600 SARS-CoV-II (94). In line with our study, absence of one of the two TPCs severely interfered with
601 infection (92, 93).
602 TPC-dependent Ca^{2+} liberation was shown to induce exocytosis, for instance, during release of cytolytic
603 granules from T cells (95) or during secretion of insulin (96). Our observations suggest that TPC1 is
604 also involved in exocytosis of lysosomes, since exogenous addition of a bacterial SMase immediately
605 before infection rescued the invasion defect in TPC1 and Syt7 K.O. cells (**Figure 2**, P) indicating that
606 reduced invasion results from a decreased delivery of ASM to the host cell surface. Thus, NAADP-
607 dependent Ca^{2+} liberation from lysosomal stores mediates Syt7-dependent fusion of lysosomes with the
608 plasma membrane resulting in the release of ASM (**Figure 6**, F). While ionomycin treatment led to
609 exocytosis of all "releasable" lysosomes, infection with *S. aureus* led to lysosomal exocytosis of only
610 ~30% of the ionomycin control (**Figure 2**, C), suggesting that *S. aureus* likely triggers local lysosomal
611 exocytosis predominantly at host-bacteria contact sites, whereas ionomycin acts globally on all cells. A
612 similar scenario has been observed for exocytosis of cytolytic granules in T lymphocytes, which differed
613 between TPC/NAADP- and ionomycin-induction (95).
614 The conversion of SM to ceramide by ASM has been associated with the generation of ceramide-
615 enriched platforms, lipid microdomains which facilitate the recruitment of certain protein receptors (97,
616 98), although the existence of such microdomains is still debated (99). We previously observed the
617 interaction of *S. aureus* with several host cell surface receptors such as NRCAM or PTK7. The
618 interaction of *S. aureus* with several host receptors was reduced upon blocking ASM-dependent
619 internalization of *S. aureus* (84). It is thus tempting to speculate that accessory receptors identified in
620 this study may be recruited to bacteria-host contact sites to facilitate rapid pathogen internalization.
621 Inhibition of CD38, a known NAADP producer (56, 57), did not influence uptake of staphylococci
622 (**Supp. Figure 1**, H). By contrast, we detected a decreased invasion in cells deficient for the Toll-like
623 receptor adaptor protein SARM1, an alternative NAADP producer [**Figure 1**, D; (59)]. However, the
624 role of SARM1 in lysosomal exocytosis and ASM release requires further investigation. The impact of
625 SARM1 on internalization of *S. aureus* was rather moderate, suggesting the existence of other NAADP-
626 generating enzymes, such as the recently identified NADPH oxidases DUOX1, DUOX2, NOX1 and
627 NOX2 (60).
628 One important characteristic of the ASM-dependent internalization pathway is its velocity - taking place
629 within the initial ten minutes of an infection with *S. aureus*, during which treatment with small molecules
630 (**Figure 3**, D), as well as genetic ablation of TPC1 (**Figure 1**, C) and Syt7 (**Figure 2**, F) resulted in
631 reduction of intracellular bacteria. This was accompanied by the quick formation of *S. aureus*-containing
632 phagosomes decorated with fluorescent SM analogs (**Figure 3**, A; **Supp. Figure 4**, **Supp. Video 1**,
633 **Supp. Video 2**).
634 Neither treatment with inhibitors or enzymes nor genetic ablation blocking the rapid internalization
635 pathway abolished the bacterial invasion of host cells completely. This supports our hypothesis that

636 several concomitant host cell entry pathways exist, which is corroborated by a large number of host cell
637 receptors interacting with *S. aureus* (13, 28, 31, 33-38). This pathway exists only in certain host cell
638 types, since among the cell types, as is -for instance- illustrated by our experiments in which
639 internalization of *S. aureus* was only sensitive to ASM inhibition in endothelial (HuLEC and HuVEC)
640 and HeLa cells (**Figure 2**, G). The proportion of bacteria taken up by rapid internalization is dependent
641 on the duration of infection and is higher in early (~50-80% of all internalized bacteria 10 min p.i.)
642 compared to late infection (~15-50% of all internalized bacteria 30 min p.i.).
643 For simplicity we describe the pathway investigated in this study as "rapid" or "ASM-dependent",
644 however a clear cut between this and other pathways cannot be easily delineated. Additionally,
645 internalization factors such as host cell receptors might possess overlapping function and could be
646 involved in several pathways. In this context, ASM might simply accelerate certain internalization
647 pathways, which could also take place in a slower fashion without involvement of ASM.
648 When we blocked the rapid internalization pathway by ASM inhibitors (**Figure 4**, A, C, D; **Supp. Figure**
649 **5**, B), Vacuolin-1 (**Figure 4**, E) or by removal of surface SM (**Figure 5**, B; **Supp. Figure 5**, B, C), we
650 observed changes in both, maturation of bacteria-containing vesicles and phagosomal escape. A delayed
651 maturation of phagosomes may affect acidification of the vesicles, a property that is sensed by *S. aureus*
652 leading to expression of a different subset of virulence factors (100) and hence may alter intracellular
653 pathogenicity.
654 The bacterial SMase β-toxin originates from *S. aureus*, however, most human pathogenic *S. aureus*
655 strains including JE2, the strain we use in the present study, do not produce β-toxin, due to a genomic
656 integration of a prophage (101). Phagosomal escape of *S. aureus* only was dependent on SM on the
657 plasma membrane during invasion but not on the presence of SM within the phago-endosome (**Figure**
658 **5**, A-C; **Supp. Figure 5**, I, J). This not only corroborated that phagosomal escape of clinically relevant
659 *S. aureus* strains is independent of the bacterial SMase β-toxin (42), but also demonstrated that the
660 outcome of phagosomal escape is influenced by processes at the plasma membrane during cell entry.
661 To exclude that inhibitor or bacterial SMase treatment caused changes in phagosomal escape by
662 affecting cellular processes other than bacterial uptake, we infected untreated wildtype cells with *S.*
663 *aureus* for 10 or 30 min, respectively, and monitored phagosomal escape. Bacteria that invaded within
664 the first 10 minutes after contacting host cells ("early invaders") are predominantly ASM-dependent
665 (**Figure 3**) and demonstrated significantly less phagosomal escape (**Figure 5**, D, E). Consistently,
666 blocking the ASM-dependent pathway led to increased proportions of ASM-independent invaders,
667 which in turn resulted in higher escape rates (**Figure 4**, C-F; **Supp. Figure 5**, G). Intracellular *S. aureus*
668 infections thus are directly influenced by the mode of internalization. This ultimately resulted in lower
669 host cytotoxicity (**Figure 6**, C-E; **Supp. Figure 9**) and bacterial replication (**Figure 6**, B) when we
670 blocked the ASM-dependent invasion.
671 An uptake-related intracellular fate has been suggested for *Mycobacterium bovis* (46), *Toxoplasma*
672 *gondii* (48) or *Brucella abortus* (49). However, in these studies the host cells were either depleted from
673 cholesterol, which causes a variety of side effects (47), or internalization was artificially induced by
674 chemicals or ectopic expression of receptors, respectively.
675 Taken together, we here describe a rapid internalization pathway for *S. aureus* into human epithelial and
676 endothelial cells. Bacteria that enter the host cells via this infection route face a distinct intracellular
677 fate. Here we show, to our knowledge, for the first time that host cells within the same population can
678 be invaded by a pathogen via multiple routes and that this results in a differential infection outcome.
679 Rapid internalization may prove beneficial for pathogens in an *in vivo* setting since internalization by
680 host cells shortens the exposure to the innate immune system within a host. Interestingly, the absence of
681 ASM in *Smpd1*$^{-/-}$ mice enhanced the potency of antibiotics to clear *S. aureus* sepsis (102). It is tempting
682 to speculate that reduced host cell invasion in absence of ASM caused a prolonged exposure of the
683 pathogen to antibiotics. Several FIASMAs are already approved drugs (103), and may have future use
684 in infection treatment.

Acknowledgements:

This work was supported by the Deutsche Forschungsgemeinschaft (DFG; https://www.dfg.de) within the research training group RTG2581 (to M.F., F.Schu., B.K.) and CRC1583 (to M.F.). C.K. and C.A. are grateful to the DFG AR 376/22-1. M.R. was supported by funds of the Bavarian State Ministry of Science and the Arts and the University of Würzburg to the Graduate School of Life Sciences (GSLS), University of Würzburg. The DFG funded the Leica TCS SP5 CLSM under project code 116162193 and the BD FACSAriaIII cell sorter under project code 206080318.
We thank Sibylle Schneider-Schaulies and Thomas Rudel for valuable discussions and critically reading the manuscript, and Nadine Vollmuth as well as Christian Stigloher for scientific advice and intense discussions. We further thank Daniel Herrmann for assistance with HPLC-MS/MS measurements of sphingolipids. We are indebted to Kathrin Stelzner for conducting FACS of cell lines and generation of *S. aureus* strains. We also are grateful to Norbert Klugbauer (Freiburg, Germany) for providing TPC1/TPC2 knock-out cells. pmRFP-LC3 was a gift from Tamotsu Yoshimori (Addgene plasmid # 21075; http://n2t.net/addgene:21075; RRID:Addgene_21075, (104)). pLVTHM (105), pMD2.G and psPAX2 (unpublished) were a gift from Didier Trono (Addgene plasmids # 12247, 12259 and 12260, respectively). pLX304-Flag-APEX2-NES was a gift from Alice Ting (Addgene plasmid # 92158, (106)) and pSpCas9(BB)-p2A-GFP (PX458) (74) was a gift from Feng Zhang (Addgene plasmid # 48138; http://n2t.net/addgene:48138). Figures were created in BioRender.

Author Contributions:

M.R., M.F. conceptualized the work, designed the methodology and wrote the original draft manuscript. M.F., B.K. acquired funding. M.R. F.S., K.U., M.P., A.M., N.K., J.W., A.I., C.K., K.P., F. Schu performed the experiments; M.R., M.F. supervised the experiments. M.R., C.A., M.F. analyzed the data; all authors edited and revised the manuscript.

Declaration of interests.
Patentability of PCK310 is currently evaluated by C.K. and C.A.

712 **Materials and Methods**

713 **Table 1 Oligonucleotides used in this study**

Purpose	Name	sequence (5´→ 3´)
Gene deletion	Syt7-sgRNA2 rv	AAACATGACGTCATTGCGGCTGAG
	Syt7-sgRNA2 fw	CACCCTCAGCCGCAATGACGTCAT
	Syt7-sgRNA1 rv	AAACCACGATGAGTCCGACCGCCG
	Syt7-sgRNA1 fw	CACCCGGCGGTCGGACTCATCGTG
	TPCN1-sgRNA2 rv	AAACAGGACGGCGCTCCTCATCTT
	TPCN1-sgRNA2 fw	CACCAAGATGAGGAGCGCCGTCCT
	TPCN1-sgRNA1 rv	AAACTTCAGACCCCGTAAGTAATC
	TPCN1-sgRNA1 fw	CACCGATTACTTACGGGGTCTGAA
	SARM1-sgRNA1 rv	AAACTAGAGTCGAGCAACGGCACG
	SARM1-sgRNA1 fw	CACCCGTGCCGTTGCTCGACTCTA
	SARM1-sgRN2 rv	AAACGCACGTAGAATAGTTGGCGA
	SARM1-sgRNA2 fw	CACCTCGCCAACTATTCTACGTGC
	SMPD1-sgRNA1 fw	CACCAGCCAGGGTGTTCTCATACC
	SMPD1-sgRNA1 rv	AAACGGTATGAGAACACCCTGGCT
	SMPD1-sgRNA2 fw	CACCGTTCTTTGGCCACACTCATG
	SMPD1-sgRNA2 rv	AAACCATGAGTGTGGCCAAAGAAC
Cloning	MP-mRFP-f	GAGACTAGCCTCGAGGTTTAAACCACCATGGCCTCCTCCGAGGACGTC
	euk_mRFP-r	GGAATGCCCGGGCGCGCCGGTGGAGTGGCGGC
	infus-CWT-f	ACCGGCGCGCCCGGGCATTCCACGCCCAATACAGGTTGG
	infus-CWT-r	GAGGTTGATTATCATATGACTAGTTCACTTTATAGTTCCCCAAAG
	eYFP-rev	CTTGTTGATGGGCTCGAGCCCTTGTACAGCTCGTCCATGCCGAG
	Pm-eYFP-inf	GACTAGCCTCGAGGTTTAAACCACCATGGTGAGCAAGGGCGAGGAG
	hLysenin-infus-r	GAGGTTGATTATCATATGACTAGTTCAGCCCACCACCTCCAG
	InfReamp-f	GGCTCGAGCCCATCAACAAG
	cYFP-f	ATGGTGAGCAAGGGCGAGGAGCTG
	his1-Flag-f	CATCATCATCATCACGGAGCGGACTACAAGGATGACGACGATAAGG
	his2-Inf-f	GACTAGCCTCGAGGTTTAAACCACCATGGCACATCATCATCATCATCA CGGAGCG
	Apex-YFP-infus-r	CGCCCTTGCTCACCATCTCGAGCCGTCCAGGGTCAGGCGCTCC
	Lamp1-as	GATAGTCTGGTAGCCTGCGTGACTCC
	EF1a_fwd	TCAAGCCTCAGACAGTGGTTC
	LV-WPRE-seq	GTATCCACATAGCGTAAAAGGAGC
	IRES-eYFP-rev	GCCCTTGCTCACCATGGTTGTGGCGCGCCATTATCATCGTGTTTTTC
	LampSP-Hibit-r	GCTAATCTTCTTGAACAGCCGCCAGCCGCTCACTGCTGACGCACAATG CATGAGGC
	Inf-Hibit-LAMP-f	GTTCAAGAAGATTAGCGCAATGTTTATGGTGAAAAATGGC
	Lamp-IRES-f	GGCTACCAGACTATCTAATGAACTAGGGGTAAATTCCGCC
	PmeInfus-SPLamp-fwd	GAGACTAGCCTCGAGGTTTAAACCACCATGGCGGCCCCCGGCAGCGC
	LV-Spe-rev	GAGGTTGATTATCATATGACTAG
	cYFP-f	ATGGTGAGCAAGGGCGAGGAGCTG
	Lamp1-p2a-f	GGCTACCAGACTATCGGCAGTGGAGAGGGCAGAGGAAG
	p2a-eYFP-r	CTCGCCCTTGCTCACTGGGCCAGGATTCTCCTC

714

715 **Cell culture**

716 HeLa (ATCC CCL-2™), 16HBE14o- (kindly provided by Prof. Jan-Peter Hildebrandt, University of
717 Greifswald) and EA.hy 926 (107) were cultivated in RPMI+GlutaMAX™ medium (Gibco™, Cat. No.
718 72400054) supplemented with 10% (v/v) heat-inactivated (56°C at 30 min) fetal bovine serum (FBS,
719 Sigma Aldrich, Cat. No. F7524) and 1 mM sodium pyruvate (Gibco™, Cat.No. 11360088).
720 HuLEC-5a (ATCC CRL-3244™) and HuVEC (Gibco™, Cat. No.C01510C) were cultured in
721 MCDB131 medium (Gibco™, Cat. No. 10372019) supplemented with microvascular growth
722 supplement (Gibco™, Cat. No. S00525), 2 mM GlutaMAX™ (Gibco™, 35050061), 5 % (v/v) heat-
723 inactivated (56°C at 30 min) FBS, 2.76 µM hydrocortisone (Sigma Aldrich, Cat. No. H0888), 0.01 ng/ml
724 human epidermal growth factor (Pep Rotech, AF-100-15) and 1x Penicillin-Streptomycin (Gibco™, Cat.
725 No. 15140122).
726 HeLa
727 HuLEC and HuVEC were detached by StemPro™ Accutase™ (Gibco™, Cat. No. A1110501) and
728 seeded at the indicated density two days prior to the experiment, whereas HeLa, 16HBE14o- and EA.hy
729 926 were detached with TrypLE™ (Gibco™, Cat. No. 12604013) and seeded one day prior to the
730 experiment.
731 When experiments were to be conducted with only 1% FBS in the culture medium, the cells initially
732 were cultured in media containing 10% FBS, were shifted to media containing 2% FBS for up to three
733 days and eventually were cultivated in media with 1% FBS one day prior to the experiment.
734 **Generation of HeLa KO cell lines**
735 Generation of K.O. cell lines is based on a previous protocol (74). sgRNAs (**Table 1**) were designed
736 with the CHOPCHOP online tool (chopchop.cbu.uib.no) and synthesized as primer pairs (Sigma
737 Aldrich). After phosphorylation with T4 nucleotide kinase (ThermoFisher, Cat. No. ER0031), the
738 sgRNAs were cloned into the BbsI sites of pSpCas9(BB)-p2A-GFP (AddGene #48138, (74)) via forced
739 ligation by BbsI (ThermoFisher, Cat. No. ER1012) and T4 Nulceotide ligase (ThermoFisher, Cat. No.
740 EL0011). The constructs were then transformed in *E. coli* DH5α (ThermoFisher, Cat. No EC0112) and
741 subsequently sequence verified.
742 HeLa cells were transfected with 1 µg each of two distinct sgRNA constructs using JetPrime (Polyplus)
743 following the manufacturer's instructions. After 36-48h, cells were sorted for strong GFP expression in
744 a FACS Aria III (BD Bioscience).To isolate ASM K.O. cell lines, we included a second sorting step.
745 Therefore, the cells were incubated with 10 µM FRET probe (73) for 2 h at 37°C/5% CO_2 and sorted
746 for cells negative in FITC emission, which correlates with the cellular ASM activity. The resulting cell
747 pools were cultivated and tested for loss of expression of the respective sgRNA target by Western
748 Blotting or ASM activity assays.
749 The following antibodies were used: mouse anti-PTK7 monoclonal IgG1 (bio-techne, Cat. No.
750 MAB4499) with a horse radish peroxidase (HRP)-conjugated anti-mouse antibody (SantaCruz, Cat. No.
751 sc-516102) and rabbit anti-TPC1 polyclonal (Thermo Fisher, Cat. No. PA5-41048) or rabbit anti-
752 SARM1 monoclonal antibody (Cell Signaling Technology, Cat. No. 13022) with an HRP-conjugated
753 anti-rabbit antibody (Biozol, Cat. No. 111-035-144).
754

755 **Generation of reporter constructs**
756 *pLV-mRFP-CWT.* mRFP and the cell wall-targeting domain of lysostaphin CWT were amplified using
757 primers MP-mRFP-f and euk_mRFP-r, as well as infus-CWT-f and infus-CWT-r, respectively. As PCR
758 templates we used pmRFP-LC3 (PMID 17534139) and pLV-YFP-CWT (108). The resulting plasmid
759 was termed pLV-mRFP-CWT. The PCR products were subsequently cloned into pLVTHM (105)
760 restricted with PmeI and SpeI by InFusion cloning following the manufacturer's recommendations.
761
762 *pLV-YFP-Lysenin.* The sequence of the sphingomyelin-binding but not pore-forming earthworm toxin
763 mutant Lysenin^{W20A} (83) was synthesized by GeneArt (ThermoFisher) adapted to human codon usage

764 and with a 5' flanking region encoding a glycine-rich linker sequence. The synthesized fragment served
765 as template for subsequent PCRs.
766 Lysenin^{W20} was amplified using oligonucleotides InfReamp-f and hLysenin-infus-r (**Table 1**).
767 YFP was amplified with Pm-eYFP-inf and eYFP-rev from template pLVTHM-YFP-CWT (108). Both
768 PCR products were joined with pLVTHM vector restricted with PmeI and SpeI by InFusion cloning
769 following the manuacturer's recommendations, thereby creating pLV-YFP-Lysenin.
770
771 Constructs were transformed into *E. coli* DH5α and sequences were validated. Plasmid preparations
772 were performed using standard laboratory procedures. VSV-G-pseudotyped Lentiviral particles were
773 generated by transfecting with each lentiviral vector as well as the plasmids pMD2.G (VSV G) and
774 psPAX2 following the protocol of (105) and target cells were transduced as described previously (108).
775
776 **Bacteria culture**
777 *S. aureus* liquid cultures were either grown in 37 g/L brain heart infusion (BHI) medium (Thermo Fisher,
778 Cat. No. 237300) or in 30 g/l TSB medium (Sigma Aldrich, Cat. No. T8907). *E. coli* liquid cultures
779 were grown in LB medium [10 g/l tryptone/peptone (Roth, Cat. No. 8952.4,) 5g/l yeast extract (Roth,
780 Cat. No 2363.2), 10 g/l NaCl (Sigma Aldrich, Cat. No. S5886)].
781 For agar plates, 15 g/L agar (Otto Norwald, Cat. No. 257353), was added to either TSB (*S. aureus*) or
782 LB (E. coli).
783 Media and plates were supplemented with appropriate antibiotics [5 µg/ml erythromycin (Sigma
784 Aldrich, Cat. No. E5389), 10 µg/ml chloramphenicol (Roth, Cat. No. 3886.2), 100 ng/ml Carbenicillin
785 (Roth, Cat. No. 6344.2)].
786 Strains used in this study are listed in **Table 2**.
787

788 **Table 2 Bacterial Strains used in this study**

Strain	Remarks	Source
S. aureus 6850		(109)
S. aureus 6850 Δ*hlb*	deficient in β-toxin production	(42)
S. aureus Cowan I	NCTC 8530, isolated from septic arthritis, agr dysfunction, low expression of toxins and proteases	ATCC 12598
S. aureus JE2	MRSA, USA300	(110)
S. aureus JE2 Δ*hla*	deficient in α-toxin production	(111)
S. aureus JE2 Δ*hlb*	deficient in β-toxin production	(11)
S. aureus JE2 SarAP1 Cerulean	Constitutive expression of the fluorescence protein Cerulean	(50)
S. aureus JE2 SarAP1 mRFP	Constitutive expression of the fluorescence protein mRFP	(45)
S. aureus JE2 p*Cer*	Anhydrous tetracycline (AHT) inducible expression of Cerulean, construct published in (112) and was transduced into *S. aureus* JE2	This work
S. aureus JE2 p*Cer+hlb*	Anhydrous tetracycline (AHT) inducible expression of Cerulean and β-toxin, construct published in (112) and was transduced into *S. aureus* JE2	This work
S. aureus Cowan I *SarAP1 Cerulean*	Constitutive expression of the fluorescence protein Cerulean	This work
S. aureus 6850 SarAP1 Cerulean	Constitutive expression of the fluorescence protein Cerulean	(45)

S. aureus 6850 Δ*hlb* SarAP1 Cerulean	Constitutive expression of the fluorescence protein Cerulean	This work

789
790
791 ***S. aureus* growth curves**
792 *S. aureus* overnight cultures were grown in BHI medium, and 1 ml was centrifuged at 14,000 for 1 min.
793 Bacteria were washed thrice with DPBS and either resuspended in BHI (for amitriptyline and ARC39
794 treatment) or infection medium [MCDB131 medium (Gibco™, Cat. No. 10372019) complemented with
795 2 mM GlutaMAX™ (Gibco™, 35050061) and 10 % (v/v) heat-inactivated (56°C at 30 min) FBS, for
796 ionomycin treatment). Bacteria suspensions were diluted to OD_{600}=0.1 in the respective medium. Then,
797 400 µL per well of the suspension as well as respective blanks were transferred into a 48 well plate and
798 OD_{600} was determined every 16 min in Tecan mPlex200 microplate reader.
799
800 ***S. aureus* infections**
801 Host cells were seeded in 6 well plates ($2x10^5$ cells per well), 12 well plates ($1x10^5$ cells per well) or 24
802 well plates ($0.5x10^5$ cell per well) either one day (HeLa, EA.hy 926, 16HBE14o$^-$) or two days (HuLEC,
803 HuVEC) prior to the experiment. Host cells were washed thrice with DPBS and infection medium or
804 Ca^{2+}-free infection medium [DMEM w/o calcium (Gibco™, Cat. No. 21068028) complemented with
805 10 % (v/v) heat-inactivated (56°C at 30 min) FBS and 200 µM BAPTA (Merck Millipore, 196418)]
806 with or without 1.8 mM $CaCl_2$ (Roth, Cat. No. 5239.1) was added. If indicated, cells were pretreated
807 with compounds prior to infection (for details about treatments see **Table 1**). For experiments involving
808 blocking of receptors by antibodies, respective solvent controls were implemented (final concentrations
809 in infection medium: 0.002% (w/v) NaN_3 (Sigma Aldrich, Cat. No. S2002) 5% glycerol (Roth, Cat. No
810 3783.2) in 10% DPBS for 30 ng/ml anti-NRCAM antibody as well as 0.01 % (w/v) NaN_3 for 50 ng/ml
811 anti-CD73 and 50 ng/ml anti-MELTF antibodies.
812
813 **Table 3 Host cell treatment with various compounds**

compound	**Supplier/Cat.No.**	**preincubation time**	**removal prior to infection?**
2-APB (2-Aminoethoxydiphenylborate)	Sigma Aldrich/ D9754	75 min	removed prior to infection
8-Bromo-cADPR (8-Bromo-cyclic ADP ribose)	Biolog/065-005	75 min	present during infection
amitriptyline	Sigma Aldrich/ A8404	75 min	present during infection
ARC39	(71)	18 h, add fresh inhibitor for another 4h or as indicated	present during infection
BAPTA-AM	Merck Millipore/ 196419; (51)	25 min	removed prior to infection
BODIPY-FL™-C12-Ceramide	Santa Cruz/ sc-503923	90 min	present during infection
BODIPY-FL™-C12-Sphingomyelin	ThermoFisher/D7711	90 min	present during infection
CD38i/78c	Sigma Aldrich/ 5387630001	75 min	present during infection

Ionomycin	Sigma Aldrich/ I0634	75 min	present during infection
PCK310	To be published elsewhere, patent pending	4h or as indicated	present during infection
trans-Ned19	Sigma Aldrich/ SML2830; (55)	75 min	present during infection
Vacuolin-1	Biozol/ MCE-HY-118630	75 min	present during infection
β-toxin	Sigma Aldrich/ S8633	75 min	removed prior to infection if not indicated otherwise

814
815 An *S. aureus* overnight culture grown in BHI containing the appropriate antibiotics was diluted to an
816 OD_{600}=0.4 in the same medium. When inducible expression of genes was required for the strains *S.*
817 *aureus* JE2 p*Cer* and *S. aureus* JE2 p*Cer+hlb,* 200 ng/ml anhydrous tetracycline (AHT, AcrosOrganics,
818 233131000) was added. The culture was grown to an OD_{600}= 0.6-1.0 and 1 ml bacterial suspension was
819 harvested by centrifugation and washed twice with Dulbecco's Phosphate Buffered Saline (DPBS,
820 Gibco™, Cat. No 14190169). The bacteria were resuspended in infection medium (or Ca^{2+}-free infection
821 medium when infection was performed in absence of extracellular Ca^{2+}). The number of bacteria per ml
822 in the suspension was determined with a Thoma counting chamber and the MOI was determined. If not
823 indicated otherwise, an MOI=10 was used for infections.
824 The infection was synchronized by centrifugation 800xg/8 min/RT (end of the centrifugation: t=0). To
825 determine bacterial invasion, the infection was stopped after 30 min (unless indicated otherwise) by
826 removing extracellular bacteria with 20 µg/ml Lysostaphin (AMBI, Cat. No. AMBICINL) in infection
827 medium for 30 min. Then, host cells were washed thrice with DPBS, lysed by addition of 1 ml/well (12
828 well plate) or 0.5 ml/well (24 well plate) Millipore water and the number of bacteria in lysates was
829 determined by plating serial dilutions (10^{-1}, 10^{-2}, 10^{-3}) on TSB agar plates. Plates were incubated
830 overnight at 37 °C and colony forming units (CFU) were enumerated. To determine invasion efficiency,
831 the number of bacteria determined in tested samples were normalized to untreated controls (set to 100%).
832 For measuring invasion dynamics, the number of bacteria was either normalized to the 30 min time point
833 of untreated controls or to the corresponding time points of untreated controls.
834 If later time points in infection were investigated, infection medium containing 2 µg/ml Lysostaphin
835 was added to the cells until the indicated time.
836 For testing bacterial susceptibility to inhibitors ("survival") or adherence, Lysostaphin treatment was
837 omitted, and host cells were immediately lysed by addition of Millipore water or washed five times with
838 DPBS and subsequently lysed with Millipore water, respectively. The number of bacteria in lysates was
839 determined by CFU counting (dilutions 10^{-2}, 10^{-3}, 10^{-4}) on TSB agar plates.
840
841 **Phagosomal escape assays**
842 For phagosomal escape assays with amitriptyline, ARC39, PCK310 and β-toxin, HeLa cells expressing
843 RFP-CWT and $Lysenin^{W20A}$-YFP were infected with the indicated *S. aureus* strain as described in the
844 previous paragraph. Infections with *S. aureus* JE2 p*Cer* and *S. aureus* JE2 p*Cer+hlb* were carried out in
845 presence of 200 ng/ml AHT.
846 For phagosomal escape assays, HeLa cells expressing RFP-CWT and $Lysenin^{W20A}$-YFP were infected
847 for 10 min (early invaders) or 30 min (early and late invaders) at the indicated MOIs.
848 For the phagosomal escape assays with two *S. aureus* JE2 strains expressing different fluorescence
849 proteins, HeLa cells expressing YFP-CWT were infected with an MOI=5 of an initial *S. aureus* JE2
850 strain (*S. aureus* JE2 SarAP1 Cerulean or *S. aureus* JE2 SarAP1 mRFP). After 12 min of infection, a

851 second infection pulse was initiated by adding the second *S. aureus* JE2 strain (expressing the
852 complementary fluorescence protein, *S. aureus* JE2 SarAP1 mRFP or *S. aureus* JE2 SarAP1 Cerulean,
853 respectively) and centrifuging the bacteria on the host cells. To exclude that the type of fluorescence
854 protein expressed by the *S. aureus* strains contributes to the experimental outcome, either strain was
855 used for the first and second infection pulse (each combination: n=4).
856
857 **Phagosomal maturation assays**
858 To monitor phagosomal maturation, HeLa cells expressing mCherry-Rab5 and YFP-Rab7 or YFP-Rab7
859 and RFP-CWT were infected with *S. aureus* JE2 SarAP1 Cerulean.
860 After 3 h p.i. (unless indicated otherwise), cells were washed thrice with DPBS and fixed with 0.2%
861 glutaraldehyde (Sigma Aldrich, Cat. No. 10333) / 4% paraformaldehyde in PBS (Morphisto, Cat. No
862 11762.01000) for 30 min at RT. Then, cells were washed thrice with DPBS, stained with 5µg/ml Hoechst
863 34580 (Thermo Fisher, Cat. No. H21486) and mounted in Mowiol [24g glycerol (Roth, Cat. No. 3783.2),
864 9.6 g Mowiol®4-88 (Roth, Cat. No 0713.2), 48 ml 0.2 M TRIS-HCl pH 8.5 (Sigma Aldrich, Cat. No
865 T1503), 24 ml Millipore water].
866 Samples were imaged with a Leica TCS SP5 confocal microscope (Wetzlar, Germany; Software Leica
867 LAS AF Version 2.7.3.9723) with a 40x immersion oil objective (NA1.3) and a resolution of 1024x1024
868 pixels [Cerulean (Ex. 458 nm/Em. 460-520), YFP (Ex. 514 nm/Em. 520-570nm), mRFP/mCherry (Ex.
869 561 nm/Em.571-635nm) and Hoechst 34580 (Ex. 405 nm/Em.410-460nm). At least 10 fields of view
870 per sample were recorded.
871 Image analysis was performed in Fiji (113) using a previously described macro (112) that identifies
872 and extracts individual bacteria from images as regions of interest (ROIs, see **Supp. Figure 7**).
873 Subsequently, fluorescent intensity in every channel is measured to determine recruitment of
874 fluorescence reporters to the bacteria. Results were exported as text files and proportion of bacteria that
875 recruited individual reporters was determined with the Flowing 2 software (Turku Bioscience Center).
876 Phagosomal escape rates were determined as the proportion of CWT-positive bacteria of the total
877 number of intracellular bacteria. Similarly, the proportion of Lysenin^{W20A}-positive escape events, the
878 ratio of Lysenin^{W20A}-/CWT-positive events and all CWT-positive events was calculated.
879 To measure the proportion of bacteria that were associated with Rab5 and/or Rab7, the proportion of
880 Rab5- and/or Rab7-positive membranes around bacteria of all intracellular bacteria was determined. For
881 experiments obtained with HeLa cells expressing YFP-Rab7 and RFP-CWT, bacteria that acquired RFP-
882 CWT were removed from the dataset. Subsequently, the proportion of Rab7-positive bacteria in relation
883 to all CWT-negative intracellular bacteria was determined.
884
885 **Live cell imaging**
886 The indicated host cells were seeded one (HeLa) or two days (HuLEC) prior to the experiments in µ-
887 slide 8 well live cell chambers (ibidi, Cat. No 80826-90) with a density of $0.375x10^5$ cells per well.
888 For monitoring host cell entry, cells were washed thrice with DPBS and were then incubated for 90 min
889 in infection medium with 1 µM BODIPY-FL-C_{12}-sphingomyelin (Thermo Fisher Cat. No. D7711), 10
890 µM BODIPY-FL-C_{12}-ceramide (Santa Cruz, Cat.No. sc-503923) or 10 µM visible-range FRET probe
891 (73). Pretreatment with the FRET probe was performed in infection medium containing 1 % (v/v) FBS.
892 Then, cells were washed thrice with DPBS and imaging medium [RPMI 1640 w/o phenol red (Gibco™,
893 Cat. No. 11835030) containing 10% (v/v) heat-inactivated (56°C/30 min) FBS (Sigma Aldrich, Cat. No.
894 F7524) and 30 mM HEPES (Gibco™, Cat.No. 15630080)] applied. Samples stained with the FRET
895 probe were imaged in imaging medium containing 1% FBS and in presence of 10 µM FRET probe.
896 Samples were infected with *S. aureus* JE2 SarAP1 Cerulean (FRET probe samples) or *S. aureus* JE2
897 SarAP1 mRFP (BODIPY-FL-C12-sphingomylein/-ceramide) at an MOI=50 without synchronization
898 by centrifugation. Infection was monitored with a Leica TCS SP5 confocal microscope (Wetzlar,
899 Germany) in intervals of 1 min by recording BODIPY-FL (Ex. 496 nm/Em. 500-535 nm), mRFP (Ex.

561 nm/Em.571) FITC (Ex. 488 nm/Em. 500-560), Cerulean (Ex. 458 nm/Em. 460-520), BODIPY-TR (Ex. 594 nm/Em. 610-680) and FRET (Ex.488 nm/ Em:610-680) channels. Cells were recorded with a 40x immersion oil objective and a resolution of 2048x2048 pixels. For samples stained with the FRET probe, 20 µg/ml Lysostaphin was added 40 min p.i. to remove extracellular bacteria.
For quantification of bacteria that associate with BODIPY-FL-C_{12}-sphingomyelin/-ceramide, individual bacteria in single frames were identified, extracted as ROIs and BODIPY-FL fluorescence in ROIs was measured in Fiji (113) as described before for phagosomal escape assays. Results were extracted as text files and the proportion of bacteria associating with BODIPY-FL was determined with Flowing2 (Turku Bioscience Center).
For monitoring intracellular *S. aureus* infection, host cells were pretreated and infected with *S. aureus* JE2 SarAP1 Cerulean (HeLa RFP-CWT/Lysenin^{W20A}-YFP) or *S. aureus* JE2 SarAP1 mRFP (HuLEC) as described in "*S. aureus* infection". HuLEC additionally were treated with 1 µM BODIPY-FL-C_{12}-sphingomyelin in infection medium for 90 min and washed thrice with DPBS before the indicated treatment was applied. After extracellular bacteria were removed with 20 µg/ml lysostaphin for 30 min, imaging medium containing 2 µg/ml lysostaphin was applied and infections were monitored in intervals of 5 min (HeLa RFP-CWT) or 20 min (HuLEC). Phagosomal escape was evaluated in Fiji as described above. To determine intracellular replication, the number of bacteria was determined for each individual frame as described before (112). The number of bacteria at each time point was then normalized to the number of bacteria detected in the first frame to calculate the relative replication.

ASM and NSM activity assays

Thin layer chromatography (TLC)-based ASM/NSM activity assays were adapted from previously published protocols (72). To determine cellular ASM activity, the indicated cell lines were seeded in 24 well plates with a density of $1x10^5$ cell per well one day (HeLa, EA.hy 926, 16HBE14o$^-$) or two days (HuLEC, HuVEC) prior to the experiment. Cells were either treated with 20 µM amitriptyline or with 10 µM ARC39 for 22 h (fresh inhibitor was applied after 18h) in infection medium. Then, cells were washed thrice and lysed by addition of 100 µL per well ASM lysis buffer [250 mM NaOAc pH 5 (Roth, Cat. No 6773.2), 0.1% Nonidet® P40 substitute (AppliChem. Cat. No. A1694,0250), 1.3 mM EDTA 1.3 mM (Roth, Cat. No. 8040.2), 1x protease inhibitor cocktail (Sigma Aldrich, 11873580001)] for 15 min/4°C. Cells were scraped from the substratum and protein concentration in the resulting lysates was measured with a Pierce™ bicinchoninic acid (BCA) assay kit (Thermo Fisher, Cat. No. 23227). 1 µg of protein was incubated with 100 µL ASM lysate assay buffer [200 mM NaOAc pH 5 (Roth, Cat. No 6773.2), 0.02 % Nonidet® P40 substitute (AppliChem. Cat. No. A1694,0250), 500 mM NaCl (VWR, Cat. No. 27810.364)] containing 0.58 µM BODIPY-FL-C_{12}-Sphingomyelin (Thermo Fisher, Cat. No. D7711) for 4h at 37°C and 300 rpm.
For measuring bacterial SMase/NSM activity in *S. aureus* cultures, an overnight culture of the indicated strain was grown in BHI medium, centrifuged 14.000xg and the supernatant was sterile filtered with 0.2 µm filter. 100 µL of sterile supernatant was incubated with 100 µL NSM assay buffer [200 mM HEPES, pH 7.0 (Roth, Cat. No. 6763.3), 200 mM $MgCl_2$ (Roth, Cat.No. 2189.2), 0.05% Nonidet P-40 (AppliChem. Cat. No. A1694,0250)] for 4h/37°C/300 rpm.
The reactions were stopped by the addition of 2:1 $CHCl_3$:MeOH (Roth, Cat. No. 3313.2 and Cat. No. 8388.6). Samples were vortexed, centrifuged at 13,000 x g for 3 min and 50-100 µL of the lower organic phase were transferred to a fresh tube. Samples were completely evaporated using a SpeedVac 5301 concentrator (Eppendorf), resuspended in 10 µL 2:1 $CHCl_3$/MeOH and spotted in 2.5 µL aliquots on a TLC plate (Alugram, Xtra Sil G/UV254, 0.2 mm/silica gel 60; VWR, Cat. No. 552-1006).
Plates were developed using 80:20 $CHCl_3$:MeOH and subsequently scanned with a Typhoon 9200 Scanner (Amersham). For quantification, intensities of the lower (SM) and the upper bands (Cer) were

949 measured in Fiji (113) and activity was determined based on the reaction time, protein amount and
950 SM/Cer ratios.
951 For the flow cytometry based read out, cells seeded in a density of $0.5x10^5$ cells per well in a 24 well
952 plate either one day (HeLa, EA.hy 926, 16HBE14o$^-$) or two days (HuLEC, HuVEC) prior to the
953 experiment. Cells were treated with ARC39 and amitriptyline as described above. Then, cells were
954 washed thrice with DPBS and incubated with 10 µM FRET probe (73) for 2h in presence of the
955 inhibitors. Subsequently, cells were washed thrice, detached with TrypLE^{TM} (Gibco^{TM}, Cat. No.
956 12604013) and resuspended with 2% (v/v) FBS in DPBS. Samples were analyzed for FITC (Ex. 488
957 nm/Em. band pass 530/30 nm) and BODIPY-TR (Ex.: 561nm/ Em. band pass 695/40nm) fluorescence
958 with Attune NxT flow cytometer (Thermo Fisher, Attune Cytometric Software v5.2.0). Cell populations
959 were analyzed for FITC and BODIPY-TR mean fluorescence in Flowing 2 (Turku Bioscience Center)
960 and FITC vs. BODIPY-TR ratios were calculated to determine arbitrary probe conversion.
961
962 **Determination of β-toxin activity on living cells**
963 HeLa cells were seeded in a 24 well plate with a density of $0.5x10^5$ cells per well. Cells were incubated
964 with 1 µM BODIPY-FL-C_{12}-SM for 24h. Then, samples were washed thrice with DPBS and treated
965 with 100 ng/ml β-toxin in infection medium or left untreated for 75 min. Subsequently, cells were
966 washed thrice with DPBS, lysed with 200 µL MeOH and detached with a cell scraper. 400 µL $CHCl_3$
967 and samples were centrifuged for 5 min/25.000xg to remove cell debris. 100 µL of the sample were
968 completely evaporated using a SpeedVac 5301 concentrator (Eppendorf), resuspended in 10 µL 2:1
969 $CHCl_3$/MeOH and spotted in 2.5 µL aliquots on a TLC plate (Alugram, Xtra Sil G/UV254, 0.2 mm/silica
970 gel 60; VWR, Cat. No. 552-1006). TLC was developed with 80:20 $CHCl_3$:MeOH and scanned with a
971 Typhoon RGB scanner (Amersham). Fluorescence intensities were evaluated in Fiji and ratios ceramide
972 vs. SM were calculated.
973
974 **Construction of HiBit-SP-LAMP1-p2A-eYFP.**
975 To visualize the transient surface exposure of lysosomal membranes on the plasma membrane of
976 epithelial cells we made use of a split NanoLuc luciferase. We inserted a region encoding the 11 amino
977 acid residues encompassing HiBiT peptide of the split NanoLuc (Promega) between the signal peptide
978 and the N-terminus of mature LAMP1.
979 For that purpose, we amplified a 144 bp fragment encoding the signal peptide of LAMP1 (SP_{LAMP1},
980 PmeInfus-SPLamp-fwd & LAMP1SP-HiBiT-r), the 1.2 kb coding region of mature LAMP1 (mLAMP1,
981 Inf-HiBiT-LAMP-f & LAMP1-as) and eYFP (cYFP-f & LV-Spe-rev) via PCR using the indicated
982 primer pairs respectively and using LAMP1-YFP containing plasmid as DNA template (41). A p2A
983 peptide encoding sequence was amplified with oligonucleotides Lamp1-p2a-f and p2a-eYFP-r using
984 pspCas9 (74) as a template. As vector we used the PmeI/SpeI-restricted pLVTHM (105).
985 The resulting DNA Fragments contained overlapping ends of at least 16 bp, which were assembled by
986 an InFusion enzyme mix (Takara Biotech) according to the manufacturer 's instructions. The resulting
987 plasmid was transformed into chemically competent *E. coli* DH5α and plated on LB agar containing
988 100 µg/ml ampicillin. Colonies were inoculated, and plasmid were prepared from the resulting overnight
989 cultures using the Qiagen Plasmid Mini kit. Sequences were determined using Sanger sequencing
990 (Microsynth) thereby establishing the correct assembly of the vector. Pseudotyped lentivirus particles
991 were generated in HEK293 cells and transduction of HeLa cells was conducted following a published
992 protocol (105).
993 eYFP production in transgenic cells here served as reporter for transfection of the cells and production
994 of the SP-HiBiT-LAMP1 proportion of the fusion protein. eYFP-positive cells were FACS-sorted for
995 medium eYFP expression levels and the resulting cell pool was named HeLa SP_{LAMP}1-HiBit-LAMP1-
996 p2A-EYFP.
997

998 **Determination of externalization of lysosomal membranes using split NanoLuc biolumin-escence.**
999 For measurement of LAMP1 externalization, $4x10^4$ per well of HeLa SP_{LAMP}1-HiBit-LAMP1-p2A-
1000 EYFP, hereafter named HeLa HiBiT-LAMP1, were seeded in white flat-bottom 96 well plates (Nunc™
1001 MicroWell™ 96 Wells, Nunclon Delta-treated, Cat. No. 136101) and grown overnight yielding $8x10^4$
1002 cells at the next day. Bioluminescence was detected using the Promega Nano-Glo HiBiT Extracellular
1003 Detection Kit (Promega # N2420).
1004 For infection with *S. aureus*, bacteria from an overnight culture were diluted to an OD600 of
1005 approximately 0.5 into 10 ml TSB and grown for 1 h. In case a preincubation with inhibitors was
1006 required (e.g. as for vacuolin-1), cells were washed twice with DPBS, and inhibitors were added in
1007 indicated concentrations in a final volume of 200 µl per well.
1008 Extracellular detection reagent was prepared by mixing 4 ml extracellular buffer, 20 µl LgBit protein
1009 and 40 µl bioluminescent substrate [Promega, Cat. No. N2420]. 100 µl extracellular detection reagent
1010 was added per well and luminescence was measured five times in 2 min intervals on a TECAN Infinite
1011 Pro 200 plate reader (37 °C, attenuation: OD1, integration time 250 ms). Then, inhibitors or bacteria
1012 were added accordingly, and luminescence measurements were continued in 2 min intervals using the
1013 settings above. The relative luminescence units (RLUs) determined in samples infected with *S. aureus*
1014 were scaled to the untreated control (set to 0%) and cells treated with 1 µM ionomycin (set to 100 %).
1015 The results describe the LAMP1 externalization as proportion of all lysosomes that can be released from
1016 host cells by ionomycin treatment.
1017
1018 **Determination of cellular sphingolipid profiles via HPLC-MS/MS**
1019 HeLa wildtype or ASM K.O. cells were seeded with a density of $3.5x10^6$ cells per well in a 6-well plate.
1020 wildtype cells were treated as described in **Table 3** with 10 µM ARC39 or 20 µM amitriptyline. Then,
1021 cells were washed thrice with DPBS, lysed with 250 µL cold MeOH and detached with a cell scraper
1022 on ice. Wells were rinsed with an additional 250 µL MeOH to ensure entire sample collection.
1023 Cell suspensions were then subjected to lipid extraction using 1 mL MeOH/$CHCl_3$ (2:1, v:v) as described
1024 before (114). The extraction solvent contained C17 ceramide (C17 Cer) and d_{31}-C16 sphingomyelin
1025 (d_{31}-C16 SM) (both Avanti Polar Lipids, Alabaster, USA) as internal standards. Chromatographic
1026 separations were achieved on a 1290 Infinity II HPLC (Agilent Technologies, Waldbronn, Germany)
1027 equipped with a Poroshell 120 EC-C8 column (3.0 × 150 mm, 2.7 µm; Agilent Technologies). MS/MS
1028 analyses were carried out using a 6495C triple-quadrupole mass spectrometer (Agilent Technologies)
1029 operating in the positive electrospray ionization mode (ESI+). Cer and SM were quantified by multiple
1030 reaction monitoring (qualifier product ions in parentheses): $[M-H_2O+H]^+ \rightarrow m/z$ 264.3 (282.3) for all
1031 Cer and $[M+H]^+ \rightarrow m/z$ 184.1 (86.1) for all SM subspecies (C16, C18, C20, C22, C24 and C24:1) (114).
1032 Peak areas of Cer and SM subspecies, as determined with MassHunter Quantitative Analysis software
1033 (version 10.1, Agilent Technologies), were normalized to those of the internal standards (C17 Cer or
1034 d_{31}-C16 SM) followed by external calibration in the range of 1 fmol to 50 pmol on column.
1035
1036 **Cytotoxicity Assays**
1037 For all cytotoxicity assays, HuLEC were seeded in 24 well plates with a density of $0.5x10^5$ cells per
1038 well two days prior to the experiment. Then, cells were infected with *S. aureus* JE2 with the indicated
1039 MOI as described in "*S. aureus* infection" and cytotoxicity was determined 21 h p.i. For cytotoxicity
1040 measurements upon ionomycin treatment, cells were incubated with the indicated concentration of
1041 ionomycin in infection medium for 75 min and then, cytotoxicity assays were conducted.
1042 Lactate dehydrogenase (LDH) assay was performed with the Cytotoxicity Detection KitPLUS (LDH,
1043 Sigma Aldrich, Cat. No. 4744934001) according to manufacturer's instructions.
1044 For annexin V and 7-Aminoactinomycin D (7-AAD) assays, cells were washed thrice with DPBS,
1045 detached with 250 µL per well trypsin and resuspended in 250 µL per well staining buffer [1.7% (v/v)
1046 APC Annexin V (BD Pharmingen™, Cat. No. 550475), 1.7% (v/v) 7-AAD (BD Pharmingen™, Cat No.

1047 559925), 2% (v/v) heat-inactivated (56°C/30 min) FBS (Sigma Aldrich, Cat. No. F7524), 4 mM $CaCl_2$
1048 (Roth, Cat. No. 5239.1) in DPBS]. After incubation for 10 min/RT, cells were analyzed with an Attune
1049 NxT flow cytometer for 7-AAD (Ex. 488 nm/Em. band pass 695/40 nm) and APC (Ex. 637 nm/Em.
1050 band pass 670/14 nm). Cell populations were analyzed with Flowing2 (Turku Biosciences Center) and
1051 gates were adjusted according to untreated control cells. To determine the proportion of cells that
1052 remained attached to the substratum during the infection, the number of cells was determined based on
1053 the number of detected single cells, flow rate and sample volume.
1054
1055 **Statistical analysis**
1056 Statistical analysis was performed in GraphPad prism (V10.1.2). One-sample t-test was used for analysis
1057 of normalized data sets. Otherwise, one- or two-way ANOVA, dependent on the number of variables,
1058 was used in combination with appropriate multiple comparisons testing. Details about sample size and
1059 corresponding statistical analysis can be found in respective figure legends. All data are shown as mean
1060 ± standard deviation.
1061
1062

References

1. Y. A. Hannun, L. M. Obeid, Sphingolipids and their metabolism in physiology and disease. *Nature Reviews Molecular Cell Biology* **19**, 175-191 (2018).
2. G. van Meer, D. R. Voelker, G. W. Feigenson, Membrane lipids: where they are and how they behave. *Nat Rev Mol Cell Biol* **9**, 112-124 (2008).
3. K. Segawa, J. Suzuki, S. Nagata, Flippases and scramblases in the plasma membrane. *Cell Cycle* **13**, 2990-2991 (2014).
4. R. O. Brady, J. N. Kanfer, M. B. Mock, D. S. Fredrickson, The metabolism of sphingomyelin. II. Evidence of an enzymatic deficiency in Niemann-Pick diseae. *Proc Natl Acad Sci U S A* **55**, 366-369 (1966).
5. B. Breiden, K. Sandhoff, Acid Sphingomyelinase, a Lysosomal and Secretory Phospholipase C, Is Key for Cellular Phospholipid Catabolism. *Int J Mol Sci* **22** (2021).
6. C. Tam *et al.*, Exocytosis of acid sphingomyelinase by wounded cells promotes endocytosis and plasma membrane repair. *J Cell Biol* **189**, 1027-1038 (2010).
7. M. C. Fernandes *et al.*, Trypanosoma cruzi subverts the sphingomyelinase-mediated plasma membrane repair pathway for cell invasion. *J Exp Med* **208**, 909-921 (2011).
8. S. Peters *et al.*, Neisseria meningitidis Type IV Pili Trigger Ca(2+)-Dependent Lysosomal Trafficking of the Acid Sphingomyelinase To Enhance Surface Ceramide Levels. *Infect Immun* **87** (2019).
9. R. W. Jenkins *et al.*, Regulated Secretion of Acid Sphingomyelinase: IMPLICATIONS FOR SELECTIVITY OF CERAMIDE FORMATION*. *Journal of Biological Chemistry* **285**, 35706-35718 (2010).
10. J. Kornhuber, C. Rhein, C. P. Muller, C. Muhle, Secretory sphingomyelinase in health and disease. *Biol Chem* **396**, 707-736 (2015).
11. Krones & Rühling *et al.*, Staphylococcus aureus alpha-Toxin Induces Acid Sphingomyelinase Release From a Human Endothelial Cell Line. *Front Microbiol* **12**, 694489 (2021).
12. S. L. Schissel *et al.*, Secretory sphingomyelinase, a product of the acid sphingomyelinase gene, can hydrolyze atherogenic lipoproteins at neutral pH. Implications for atherosclerotic lesion development. *J Biol Chem* **273**, 2738-2746 (1998).
13. C. Li *et al.*, Regulation of Staphylococcus aureus Infection of Macrophages by CD44, Reactive Oxygen Species, and Acid Sphingomyelinase. *Antioxid Redox Signal* **28**, 916-934 (2018).
14. H. Grassme *et al.*, Acidic sphingomyelinase mediates entry of N. gonorrhoeae into nonphagocytic cells. *Cell* **91**, 605-615 (1997).
15. A. Carpinteiro *et al.*, Pharmacological Inhibition of Acid Sphingomyelinase Prevents Uptake of SARS-CoV-2 by Epithelial Cells. *Cell Rep Med* **1**, 100142 (2020).
16. S. Luisoni *et al.*, Co-option of Membrane Wounding Enables Virus Penetration into Cells. *Cell Host & Microbe* **18**, 75-85 (2015).
17. E. Avota, E. Gulbins, S. Schneider-Schaulies, DC-SIGN mediated sphingomyelinase-activation and ceramide generation is essential for enhancement of viral uptake in dendritic cells. *PLoS Pathog* **7**, e1001290 (2011).
18. A. Sakr, F. Brégeon, J. L. Mège, J. M. Rolain, O. Blin, Staphylococcus aureus Nasal Colonization: An Update on Mechanisms, Epidemiology, Risk Factors, and Subsequent Infections. *Front Microbiol* **9**, 2419 (2018).
19. L. F. McCaig, L. C. McDonald, S. Mandal, D. B. Jernigan, Staphylococcus aureus-associated skin and soft tissue infections in ambulatory care. *Emerg Infect Dis* **12**, 1715-1723 (2006).
20. L. Liesenborghs *et al.*, Staphylococcus aureus endocarditis: distinct mechanisms of bacterial adhesion to damaged and inflamed heart valves. *Eur Heart J* **40**, 3248-3259 (2019).
21. J. A. Silversides, E. Lappin, A. J. Ferguson, Staphylococcal toxic shock syndrome: mechanisms and management. *Curr Infect Dis Rep* **12**, 392-400 (2010).
22. C. Antimicrobial Resistance, Global burden of bacterial antimicrobial resistance in 2019: a systematic analysis. *Lancet* **399**, 629-655 (2022).
23. M. Fraunholz, B. Sinha, Intracellular Staphylococcus aureus: live-in and let die. *Front Cell Infect Microbiol* **2**, 43 (2012).

24. I. Rodrigues Lopes *et al.*, Microscopy-based phenotypic profiling of infection by Staphylococcus aureus clinical isolates reveals intracellular lifestyle as a prevalent feature. *Nature Communications* **13**, 7174 (2022).
25. J. W. Hommes, B. G. J. Surewaard, Intracellular Habitation of Staphylococcus aureus: Molecular Mechanisms and Prospects for Antimicrobial Therapy. *Biomedicines* **10**, 1804 (2022).
26. S. N. Qazi, S. E. Harrison, T. Self, P. Williams, P. J. Hill, Real-time monitoring of intracellular Staphylococcus aureus replication. *J Bacteriol* **186**, 1065-1077 (2004).
27. J. Abel *et al.*, Staphylococcus aureus evades the extracellular antimicrobial activity of mast cells by promoting its own uptake. *J Innate Immun* **3**, 495-507 (2011).
28. B. Sinha *et al.*, Fibronectin-binding protein acts as Staphylococcus aureus invasin via fibronectin bridging to integrin alpha5beta1. *Cell Microbiol* **1**, 101-117 (1999).
29. F. Agerer *et al.*, Cellular invasion by Staphylococcus aureus reveals a functional link between focal adhesion kinase and cortactin in integrin-mediated internalisation. *J Cell Sci* **118**, 2189-2200 (2005).
30. F. Agerer, A. Michel, K. Ohlsen, C. R. Hauck, Integrin-mediated invasion of Staphylococcus aureus into human cells requires Src family protein-tyrosine kinases. *J Biol Chem* **278**, 42524-42531 (2003).
31. Y. T. Ying *et al.*, Annexin A2-Mediated Internalization of Staphylococcus aureus into Bovine Mammary Epithelial Cells Requires Its Interaction with Clumping Factor B. *Microorganisms* **9** (2021).
32. S. L. Stroschein-Stevenson, E. Foley, P. H. O'Farrell, A. D. Johnson, Identification of Drosophila gene products required for phagocytosis of Candida albicans. *PLoS Biol* **4**, e4 (2006).
33. A. M. Towell *et al.*, Staphylococcus aureus binds to the N-terminal region of corneodesmosin to adhere to the stratum corneum in atopic dermatitis. *Proceedings of the National Academy of Sciences* **118**, e2014444118 (2021).
34. F. Askarian *et al.*, The interaction between Staphylococcus aureus SdrD and desmoglein 1 is important for adhesion to host cells. *Scientific Reports* **6**, 22134 (2016).
35. N. Bravo-Santano *et al.*, Host-directed kinase inhibitors act as novel therapies against intracellular Staphylococcus aureus. *Scientific Reports* **9**, 4876 (2019).
36. P. M. Tribelli *et al.*, Staphylococcus aureus Lpl protein triggers human host cell invasion via activation of Hsp90 receptor. *Cell Microbiol* **22**, e13111 (2020).
37. N. Hirschhausen *et al.*, A novel staphylococcal internalization mechanism involves the major autolysin Atl and heat shock cognate protein Hsc70 as host cell receptor. *Cell Microbiol* **12**, 1746-1764 (2010).
38. K. Dziewanowska *et al.*, Staphylococcal fibronectin binding protein interacts with heat shock protein 60 and integrins: role in internalization by epithelial cells. *Infect Immun* **68**, 6321-6328 (2000).
39. A. Moldovan, M. J. Fraunholz, In or out: Phagosomal escape of Staphylococcus aureus. *Cell Microbiol* **21**, e12997 (2019).
40. C. E. Jauregui, J. P. Mansell, M. A. Jepson, H. F. Jenkinson, Differential interactions of Streptococcus gordonii and Staphylococcus aureus with cultured osteoblasts. *Mol Oral Microbiol* **28**, 250-266 (2013).
41. B. Giese *et al.*, Staphylococcal alpha-toxin is not sufficient to mediate escape from phagolysosomes in upper-airway epithelial cells. *Infect Immun* **77**, 3611-3625 (2009).
42. M. Grosz *et al.*, Cytoplasmic replication of Staphylococcus aureus upon phagosomal escape triggered by phenol-soluble modulin alpha. *Cell Microbiol* **16**, 451-465 (2014).
43. J. Horn, K. Stelzner, T. Rudel, M. Fraunholz, Inside job: Staphylococcus aureus host-pathogen interactions. *Int J Med Microbiol* **308**, 607-624 (2018).
44. R. Wang *et al.*, Identification of novel cytolytic peptides as key virulence determinants for community-associated MRSA. *Nat Med* **13**, 1510-1514 (2007).
45. K. Stelzner *et al.*, Intracellular Staphylococcus aureus employs the cysteine protease staphopain A to induce host cell death in epithelial cells. *PLoS Pathog* **17**, e1009874 (2021).

46. J. Gatfield, J. Pieters, Essential role for cholesterol in entry of mycobacteria into macrophages. *Science* **288**, 1647-1650 (2000).
47. R. Zidovetzki, I. Levitan, Use of cyclodextrins to manipulate plasma membrane cholesterol content: evidence, misconceptions and control strategies. *Biochim Biophys Acta* **1768**, 1311-1324 (2007).
48. K. A. Joiner, S. A. Fuhrman, H. M. Miettinen, L. H. Kasper, I. Mellman, Toxoplasma gondii: Fusion Competence of Parasitophorous Vacuoles in Fc Receptor-Transfected Fibroblasts. *Science* **249**, 641-646 (1990).
49. S. Kim, M. Watarai, S.-i. Makino, T. Shirahata, Membrane sorting during swimming internalization of Brucella is required for phagosome trafficking decisions. *Microbial Pathogenesis* **33**, 225-237 (2002).
50. K. Stelzner *et al.*, Intracellular Staphylococcus aureus Perturbs the Host Cell Ca(2+) Homeostasis To Promote Cell Death. *mBio* **11** (2020).
51. R. Y. Tsien, A non-disruptive technique for loading calcium buffers and indicators into cells. *Nature* **290**, 527-528 (1981).
52. M. D. Bootman, G. Bultynck, Fundamentals of Cellular Calcium Signaling: A Primer. *Cold Spring Harb Perspect Biol* **12** (2020).
53. T. Maruyama, T. Kanaji, S. Nakade, T. Kanno, K. Mikoshiba, 2APB, 2-aminoethoxydiphenyl borate, a membrane-penetrable modulator of Ins(1,4,5)P3-induced Ca2+ release. *J Biochem* **122**, 498-505 (1997).
54. T. F. Walseth, H. C. Lee, Synthesis and characterization of antagonists of cyclic-ADP-ribose-induced Ca2+ release. *Biochim Biophys Acta* **1178**, 235-242 (1993).
55. E. Naylor *et al.*, Identification of a chemical probe for NAADP by virtual screening. *Nature Chemical Biology* **5**, 220-226 (2009).
56. S. Y. Kim, B. H. Cho, U. H. Kim, CD38-mediated Ca2+ signaling contributes to angiotensin II-induced activation of hepatic stellate cells: attenuation of hepatic fibrosis by CD38 ablation. *J Biol Chem* **285**, 576-582 (2010).
57. S. Y. Rah, M. Mushtaq, T. S. Nam, S. H. Kim, U. H. Kim, Generation of cyclic ADP-ribose and nicotinic acid adenine dinucleotide phosphate by CD38 for Ca2+ signaling in interleukin-8-treated lymphokine-activated killer cells. *J Biol Chem* **285**, 21877-21887 (2010).
58. Z. L. Piedra-Quintero, Z. Wilson, P. Nava, M. Guerau-de-Arellano, CD38: An Immunomodulatory Molecule in Inflammation and Autoimmunity. *Front Immunol* **11**, 597959 (2020).
59. C. Angeletti *et al.*, SARM1 is a multi-functional NAD(P)ase with prominent base exchange activity, all regulated bymultiple physiologically relevant NAD metabolites. *iScience* **25**, 103812 (2022).
60. F. Gu *et al.*, Dual NADPH oxidases DUOX1 and DUOX2 synthesize NAADP and are necessary for Ca(2+) signaling during T cell activation. *Sci Signal* **14**, eabe3800 (2021).
61. E. V. Caler, S. Chakrabarti, K. T. Fowler, S. Rao, N. W. Andrews, The Exocytosis-regulatory protein synaptotagmin VII mediates cell invasion by Trypanosoma cruzi. *J Exp Med* **193**, 1097-1104 (2001).
62. H. Grassmé, A. Riehle, B. Wilker, E. Gulbins, Rhinoviruses infect human epithelial cells via ceramide-enriched membrane platforms. *J Biol Chem* **280**, 26256-26262 (2005).
63. M. E. Miller, S. Adhikary, A. A. Kolokoltsov, R. A. Davey, Ebolavirus Requires Acid Sphingomyelinase Activity and Plasma Membrane Sphingomyelin for Infection. *Journal of Virology* **86**, 7473-7483 (2012).
64. M. P. Hall *et al.*, Engineered Luciferase Reporter from a Deep Sea Shrimp Utilizing a Novel Imidazopyrazinone Substrate. *ACS Chemical Biology* **7**, 1848-1857 (2012).
65. A. S. Dixon *et al.*, NanoLuc Complementation Reporter Optimized for Accurate Measurement of Protein Interactions in Cells. *ACS Chemical Biology* **11**, 400-408 (2016).
66. N. W. Andrews, "Detection of Lysosomal Exocytosis by Surface Exposure of Lamp1 Luminal Epitopes" in Lysosomes: Methods and Protocols, K. Öllinger, H. Appelqvist, Eds. (Springer New York, New York, NY, 2017), 10.1007/978-1-4939-6934-0_13, pp. 205-211.

67. A. Rodriguez, P. Webster, J. Ortego, N. W. Andrews, Lysosomes behave as Ca2+-regulated exocytic vesicles in fibroblasts and epithelial cells. *J Cell Biol* **137**, 93-104 (1997).
68. J. Cerny *et al.*, The small chemical vacuolin-1 inhibits Ca(2+)-dependent lysosomal exocytosis but not cell resealing. *EMBO Rep* **5**, 883-888 (2004).
69. A. Reddy, E. V. Caler, N. W. Andrews, Plasma membrane repair is mediated by Ca(2+)-regulated exocytosis of lysosomes. *Cell* **106**, 157-169 (2001).
70. H. Grassmé *et al.*, Acidic sphingomyelinase mediates entry of N. gonorrhoeae into nonphagocytic cells. *Cell* **91**, 605-615 (1997).
71. A. G. Roth *et al.*, Potent and selective inhibition of acid sphingomyelinase by bisphosphonates. *Angew Chem Int Ed Engl* **48**, 7560-7563 (2009).
72. C. Muhle, J. Kornhuber, Assay to measure sphingomyelinase and ceramidase activities efficiently and safely. *J Chromatogr A* **1481**, 137-144 (2017).
73. C. Kappe, Z. H. Mohamed, E. Naser, A. Carpinteiro, C. Arenz, A Novel Visible Range FRET Probe for Monitoring Acid Sphingomyelinase Activity in Living Cells. *Chemistry* **26**, 5780-5783 (2020).
74. F. A. Ran *et al.*, Genome engineering using the CRISPR-Cas9 system. *Nature Protocols* **8**, 2281-2308 (2013).
75. S. M. Hammad *et al.*, Blood sphingolipidomics in healthy humans: impact of sample collection methodology. *Journal of Lipid Research* **51**, 3074-3087 (2010).
76. C. Muhle *et al.*, Characterization of acid sphingomyelinase activity in human cerebrospinal fluid. *PLoS One* **8**, e62912 (2013).
77. E. H. Schuchman, R. J. Desnick, Types A and B Niemann-Pick disease. *Mol Genet Metab* **120**, 27-33 (2017).
78. C. Hoffmann *et al.*, Caveolin limits membrane microdomain mobility and integrin-mediated uptake of fibronectin-binding pathogens. *J Cell Sci* **123**, 4280-4291 (2010).
79. L.-P. Tricou *et al.*, Staphylococcus aureus can use an alternative pathway to be internalized by osteoblasts in absence of β1 integrins. *Scientific Reports* **14**, 28643 (2024).
80. J. Rappaport, C. Garnacho, S. Muro, Clathrin-mediated endocytosis is impaired in type A-B Niemann-Pick disease model cells and can be restored by ICAM-1-mediated enzyme replacement. *Mol Pharm* **11**, 2887-2895 (2014).
81. J. Rappaport, R. L. Manthe, C. Garnacho, S. Muro, Altered Clathrin-Independent Endocytosis in Type A Niemann-Pick Disease Cells and Rescue by ICAM-1-Targeted Enzyme Delivery. *Mol Pharm* **12**, 1366-1376 (2015).
82. M. Rühling *et al.*, Trifunctional sphingomyelin derivatives enable nanoscale resolution of sphingomyelin turnover in physiological and infection processes via expansion microscopy. *Nature Communications* **15**, 7456 (2024).
83. C. J. Ellison, W. Kukulski, K. B. Boyle, S. Munro, F. Randow, Transbilayer Movement of Sphingomyelin Precedes Catastrophic Breakage of Enterobacteria-Containing Vacuoles. *Curr Biol* **30**, 2974-2983 e2976 (2020).
84. M. Rühling, F. Schmelz, A. Kempf, K. Paprotka, J. Fraunholz Martin, Identification of the Staphylococcus aureus endothelial cell surface interactome by proximity labeling. *mBio* **0**, e03654-03624 (2025).
85. F. Falugi, H. K. Kim, D. M. Missiakas, O. Schneewind, Role of protein A in the evasion of host adaptive immune responses by Staphylococcus aureus. *mBio* **4**, e00575-00513 (2013).
86. A. J. Morgan, R. Jacob, Ionomycin enhances Ca2+ influx by stimulating store-regulated cation entry and not by a direct action at the plasma membrane. *Biochem J* **300 (Pt 3)**, 665-672 (1994).
87. O. Sano *et al.*, Vacuolin-1 inhibits autophagy by impairing lysosomal maturation via PIKfyve inhibition. *FEBS Letters* **590**, 1576-1585 (2016).
88. J.-S. Schonn, A. Maximov, Y. Lao, T. C. Südhof, J. B. Sørensen, Synaptotagmin-1 and -7 are functionally overlapping Ca²⁺ sensors for exocytosis in adrenal chromaffin cells. *Proceedings of the National Academy of Sciences* **105**, 3998-4003 (2008).
89. D. Shen *et al.*, Lipid storage disorders block lysosomal trafficking by inhibiting a TRP channel and lysosomal calcium release. *Nat Commun* **3**, 731 (2012).

1273 90. L. C. Davis, A. J. Morgan, A. Galione, NAADP-regulated two-pore channels drive phagocytosis
1274 through endo-lysosomal Ca(2+) nanodomains, calcineurin and dynamin. *EMBO J* **39**, e104058
1275 (2020).
1276 91. A. J. Morgan, F. M. Platt, E. Lloyd-Evans, A. Galione, Molecular mechanisms of endolysosomal
1277 Ca2+ signalling in health and disease. *Biochemical Journal* **439**, 349-378 (2011).
1278 92. Y. Sakurai *et al.*, Ebola virus. Two-pore channels control Ebola virus host cell entry and are drug
1279 targets for disease treatment. *Science* **347**, 995-998 (2015).
1280 93. G. S. Gunaratne, Y. Yang, F. Li, T. F. Walseth, J. S. Marchant, NAADP-dependent Ca(2+) signaling
1281 regulates Middle East respiratory syndrome-coronavirus pseudovirus translocation through
1282 the endolysosomal system. *Cell Calcium* **75**, 30-41 (2018).
1283 94. X. Ou *et al.*, Characterization of spike glycoprotein of SARS-CoV-2 on virus entry and its immune
1284 cross-reactivity with SARS-CoV. *Nature Communications* **11**, 1620 (2020).
1285 95. L. C. Davis *et al.*, NAADP activates two-pore channels on T cell cytolytic granules to stimulate
1286 exocytosis and killing. *Curr Biol* **22**, 2331-2337 (2012).
1287 96. A. Arredouani *et al.*, Nicotinic Acid Adenine Dinucleotide Phosphate (NAADP) and
1288 Endolysosomal Two-pore Channels Modulate Membrane Excitability and Stimulus-Secretion
1289 Coupling in Mouse Pancreatic β Cells. *J Biol Chem* **290**, 21376-21392 (2015).
1290 97. C. R. Bollinger, V. Teichgräber, E. Gulbins, Ceramide-enriched membrane domains. *Biochimica*
1291 *et Biophysica Acta (BBA) - Molecular Cell Research* **1746**, 284-294 (2005).
1292 98. Y. Zhang, X. Li, K. A. Becker, E. Gulbins, Ceramide-enriched membrane domains—Structure and
1293 function. *Biochimica et Biophysica Acta (BBA) - Biomembranes* **1788**, 178-183 (2009).
1294 99. I. Levental, K. R. Levental, F. A. Heberle, Lipid Rafts: Controversies Resolved, Mysteries Remain.
1295 *Trends Cell Biol* **30**, 341-353 (2020).
1296 100. R. S. Flannagan, R. C. Kuiack, M. J. McGavin, D. E. Heinrichs, Staphylococcus aureus Uses the
1297 GraXRS Regulatory System To Sense and Adapt to the Acidified Phagolysosome in
1298 Macrophages. *mBio* **9** (2018).
1299 101. R. Pantůcek *et al.*, Identification of bacteriophage types and their carriage in Staphylococcus
1300 aureus. *Arch Virol* **149**, 1689-1703 (2004).
1301 102. H. Peng *et al.*, Acid sphingomyelinase inhibition protects mice from lung edema and lethal
1302 Staphylococcus aureus sepsis. *J Mol Med (Berl)* **93**, 675-689 (2015).
1303 103. J. Kornhuber *et al.*, Functional Inhibitors of Acid Sphingomyelinase (FIASMAs): a novel
1304 pharmacological group of drugs with broad clinical applications. *Cell Physiol Biochem* **26**, 9-20
1305 (2010).
1306 104. S. Kimura, T. Noda, T. Yoshimori, Dissection of the autophagosome maturation process by a
1307 novel reporter protein, tandem fluorescent-tagged LC3. *Autophagy* **3**, 452-460 (2007).
1308 105. M. Wiznerowicz, D. Trono, Conditional suppression of cellular genes: lentivirus vector-
1309 mediated drug-inducible RNA interference. *J Virol* **77**, 8957-8961 (2003).
1310 106. V. Hung *et al.*, Proteomic mapping of cytosol-facing outer mitochondrial and ER membranes in
1311 living human cells by proximity biotinylation. *eLife* **6**, e24463 (2017).
1312 107. C. J. Edgell, C. C. McDonald, J. B. Graham, Permanent cell line expressing human factor VIII-
1313 related antigen established by hybridization. *Proceedings of the National Academy of Sciences*
1314 **80**, 3734-3737 (1983).
1315 108. S. Blättner *et al.*, Staphylococcus aureus Exploits a Non-ribosomal Cyclic Dipeptide to Modulate
1316 Survival within Epithelial Cells and Phagocytes. *PLOS Pathogens* **12**, e1005857 (2016).
1317 109. J. M. Vann, R. A. Proctor, Ingestion of Staphylococcus aureus by bovine endothelial cells results
1318 in time- and inoculum-dependent damage to endothelial cell monolayers. *Infect Immun* **55**,
1319 2155-2163 (1987).
1320 110. P. D. Fey *et al.*, A genetic resource for rapid and comprehensive phenotype screening of
1321 nonessential *Staphylococcus aureus* genes. *MBio* **4**, e00537-00512 (2013).
1322 111. K. A. Becker *et al.*, Staphylococcus aureus Alpha-Toxin Disrupts Endothelial-Cell Tight Junctions
1323 via Acid Sphingomyelinase and Ceramide. *Infect Immun* **86** (2018).

112. B. Giese *et al.*, Expression of δ-toxin by Staphylococcus aureus mediates escape from phago-endosomes of human epithelial and endothelial cells in the presence of β-toxin. *Cell Microbiol* **13**, 316-329 (2011).
113. J. Schindelin *et al.*, Fiji: an open-source platform for biological-image analysis. *Nat Methods* **9**, 676-682 (2012).
114. A. Prell, D. Wigger, A. Huwiler, F. Schumacher, B. Kleuser, The sphingosine kinase 2 inhibitors ABC294640 and K145 elevate (dihydro)sphingosine 1-phosphate levels in various cells. *J Lipid Res* **65**, 100631 (2024).

Supplementary Figures

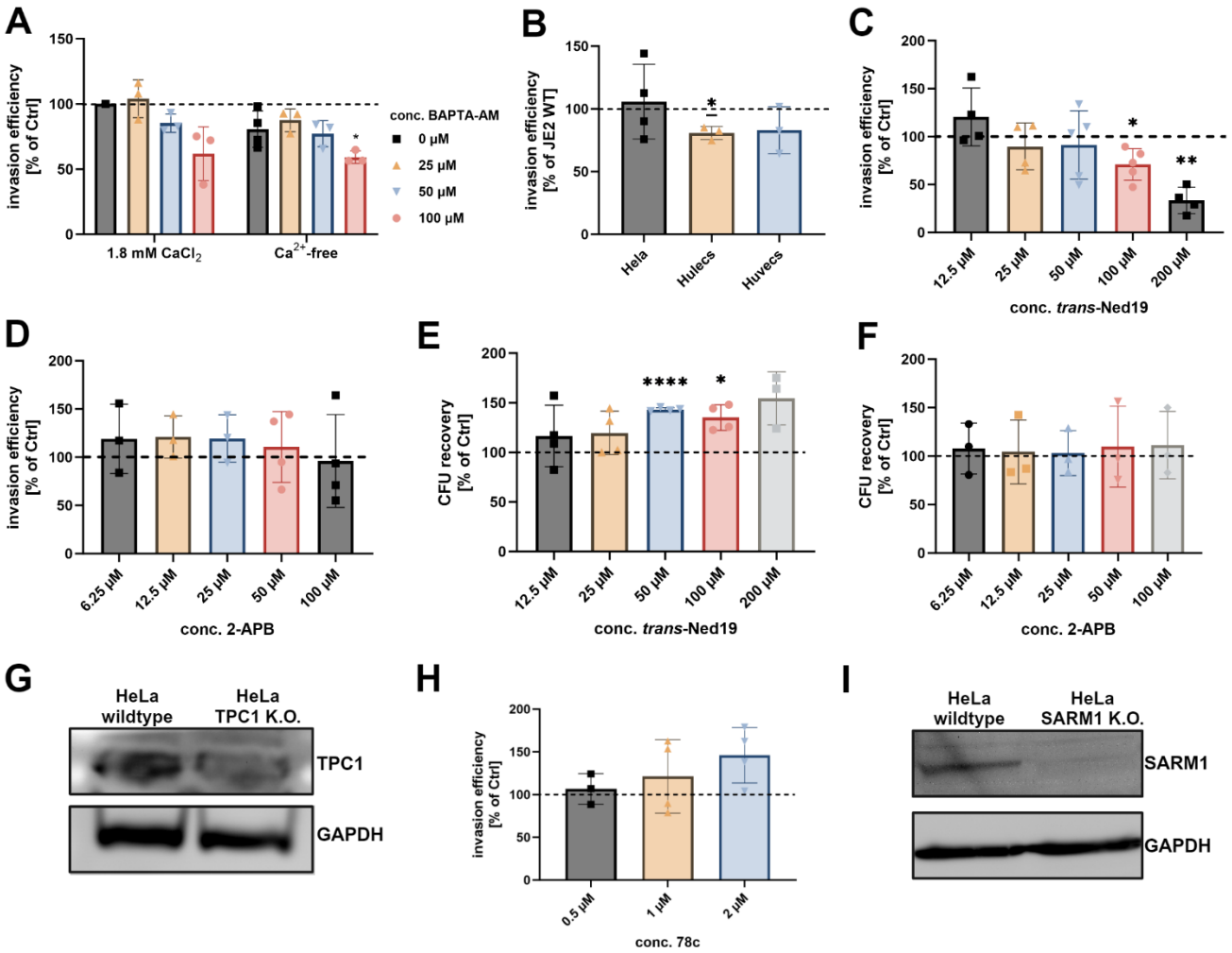

Supp. Figure 1 Supporting information for Ca^{2+}-dependent internalization of *S. aureus*.
. (**A) Chelation of intracellular but not presence of extracellular Ca^{2+} affects *S. aureus* internalization by HeLa cells.** HeLa cells were preloaded with varying concentrations of the cell-permeable Ca^{2+} chelator BAPTA-AM and then infected with *S. aureus* JE2 in presence (+1.8 mM $CaCl_2$) or absence (Ca^{2+}-free) of Ca^{2+} in the cell culture medium. Invasion efficiency was determined by CFU plating. (**B) α-toxin plays only a subordinate role during *S. aureus* uptake by host cells.** HeLa, HuLEC or HuVEC were infected with *S. aureus* JE2 wildtype or a strain deficient in α-toxin production (Δ*hla*). Invasion efficiency was determined by CFU plating. The number of intracellular bacteria was normalized to samples infected with the wildtype. **(C, D) *trans*-Ned19 but not 2-APB affects invasion of *S. aureus* JE2 in HeLa.** HeLa cells were pre-treated with *trans*-Ned19 (**C**) or 2-APB (**D**). 2-APB was removed from the cells shortly before infection to avoid direct contact of inhibitor and bacteria (due to a bactericidal effect of 2-APB; data not shown). Then, cells were infected with *S. aureus* JE2 and invasion efficiency was determined. **(E, F) *trans*-Ned19 and 2-APB have no effect on *S. aureus* JE2 in our infection protocol.** HeLa cells were pre-treated with or 2-APB (**E**) or *trans*-Ned19 (**F**). 2-APB was removed from the cells shortly before infection. Then, cells were infected with *S. aureus* JE2 and, after 30 min, total bacteria (extra- and intracellular) were recovered by CFU plating. (**G) Reduction of TPC1 expression in a Cas9-treated cell pool (HeLa TPC1 K.O.).** TPC1 as well as GAPDH (loading control) was detected in lysates of wildtype and TPC1 K.O. cells via Western blot. **(H) CD38 is not involved in *S. aureus* internalization.** HeLa cells were pretreated with the CD38 inhibitor 78c and invasion efficiency of *S. aureus* JE2 was determined. (**I) Reduction of SARM1 expression in a Cas9-treated cell pool (HeLa SARM1 K.O.).** TPC1 as well as GAPDH (loading control) was detected in lysates of wildtype and SARM1 K.O. cells via Western blot. Statistics: one sample t-test, Bars represent mean +/- SD. *p≤0.05, **p≤0.01, ***p≤0.001, ****p≤0.0001.

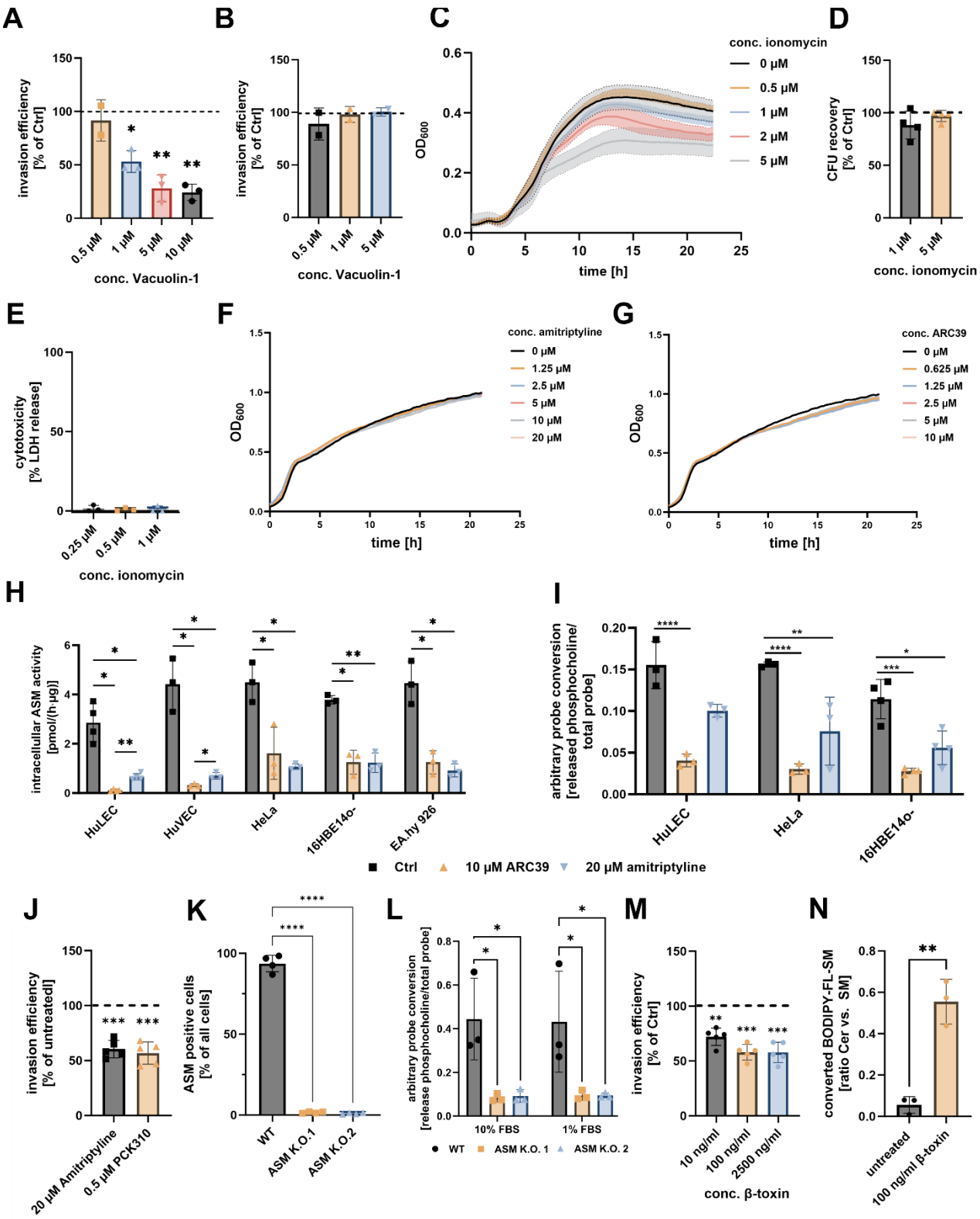

Supp. Figure 2 Supporting information for the involvement of lysosomal exocytosis and ASM in *S. aureus* invasion

(A) High ionomycin concentrations interfere with growth of *S. aureus* JE2. *S. aureus* JE2 was grown in in presence of varying concentrations of ionomycin. Growth (OD_{600}) was determined in a microplate reader. **(B) Ionomycin does not affect survival of *S. aureus* JE2 during infection of host cells.** HeLa cells were pretreated with varying concentrations of ionomycin and subsequently, infected with *S. aureus* JE2. After 30 min, cells were lysed and surviving extra- and intracellular bacteria were recovered by CFU count. **(C) Ionomycin does not affect host cell survival.** HeLa cells were treated with the indicated concentrations of ionomycin, and cytotoxicity was determined by measuring in lactate dehydrogenase (LDH) release. **(D)**

Blocking lysosomal exocytosis by Vacuolin-1 reduces *S. aureus* invasion in HeLa. HeLa cells were treated with increasing concentrations of the lysosomal exocytosis inhibitor Vacuolin-1. The invasion efficiency of *S. aureus* JE2 was determined 30 min p.i. **(E) Vacuolin-1 has no bactericidal effect.** HeLa cells were treated with Vacuolin-1 and infected with *S. aureus* JE2. After 30 min, total bacteria (extra- and intracellular) were recovered by CFU plating and normalized to untreated controls. **(F, G) The ASM inhibitors amitriptyline and ARC39 have no effect on growth of *S. aureus*.** *S. aureus* JE2 was grown in presence of varying concentrations of amitriptyline (**F**) or ARC39 (**G**) in BHI medium and growth was determined by measuring OD_{600} in a microplate reader. **(H, I) ASM activity and ASM inhibition by ARC39 and amitriptyline are similar among human cell lines.** Several cell lines were treated with amitriptyline or ARC39 and ASM activity within cell lysates was assessed by either thin layer chromatography-based ASM activity assays, detecting the conversion of BODIPY-C12-SM (**H**), or by a flow cytometry-based ASM activity assay and conversion of visible-range FRET probe (**I**). **(J) Microscopy-based measurement of invasion efficiency in amitriptyline- and PCK310-treated Hela cells.** Hela cells were treated with 20 µM amitriptyline (75 min) or 0.5 µM PCK310 (4h) and infected with *S. aureus* JE2 expressing Cerulean. Number of intracellular bacteria per host cell was determined by CLSM. n=5. **(K) Validation of ASM K.O. cell pools.** ASM activity in HeLa wildytpe or ASM K.O.s was determined with the visible-range FRET probe and flow cytometry. The proportion of ASM-positive cells in the cell population was determined. n=4. **(L) FBS concentration in culture medium does not affect cell-associated ASM activity in ASM K.O. cell lines.** HeLa WT or ASM K.O. cells were cultured in 1% or 10% FBS and cellular ASM activity was determined with a visible range FRET probe by flow cytometry. n=3. **(M) Removal of SM from the plasma membrane by β-toxin affects *S. aureus* host cell entry in HeLa.** HeLa cells were pretreated with the indicated concentrations of β-toxin and subsequently the invasion efficiency of *S. aureus* JE2 was determined. **(N) Treatment of HeLa with the bacterial SMases β-toxin results in generation of ceramide.** HeLa cells were preloaded with 1 µM BODIPY-FL-C_{12}-SM and treated with β-toxin for 75 min. Quantities of ceramide and SM were determined by TLC and ratio of ceramide vs. SM were calculated. Statistics: one sample t-test (D, J, M), mixed-effects model (REML) and Tukey`s multiple comparison (H, I), one-way ANOVA and Dunnett`s multiple comparison (K), two-way ANOVA and Šídák's multiple comparison (L), unpaired Student´s t-test (N). Bars represent mean +/- SD. *$p \leq 0.05$, **$p \leq 0.01$, ***$p \leq 0.001$, ****$p \leq 0.0001$.

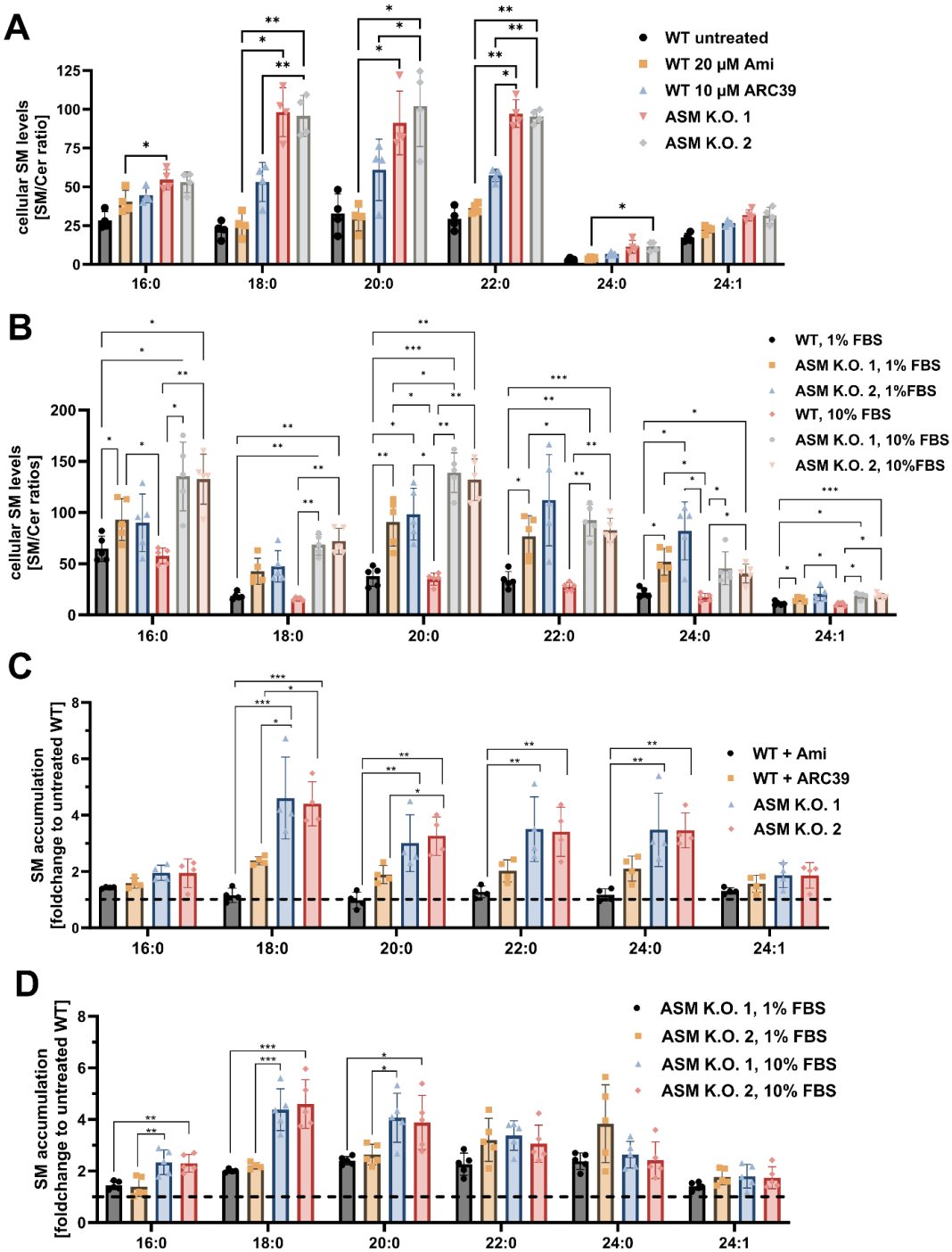

Supp. Figure 3 Effects of genetic K.O. and inhibition of ASM on cellular SM levels.
HeLa WT or two ASM-depleted HeLa cells pools (ASM K.O. 1 and 2) were cultured in medium containing 10% or, if indicated, 1% FBS. If indicated WT cells were exposed to 20 µM amitriptyline for 75 min, or to 10 µM ARC39 for 22h. Amounts of SM and Cer species with different acyl chain lengths were quantified by HPLC-MS/MS and SM/Cer ratios were calculated to determine the cellular SM levels (A and B). To assess SM accumulation upon K.O. or inhibitor treatment, SM levels were normalized to untreated WT cells (set to 1, C and D). n≥4. Statistics: Two-way ANOVA and Tukey's multiple comparison (A, B) and One-way ANOVA with Tukey's multiple comparison

for individual acyl chain lengths (C, D). Bars represent mean +/- SD. *p≤0.05, **p≤0.01, ***p≤0.001, ****p≤0.0001.

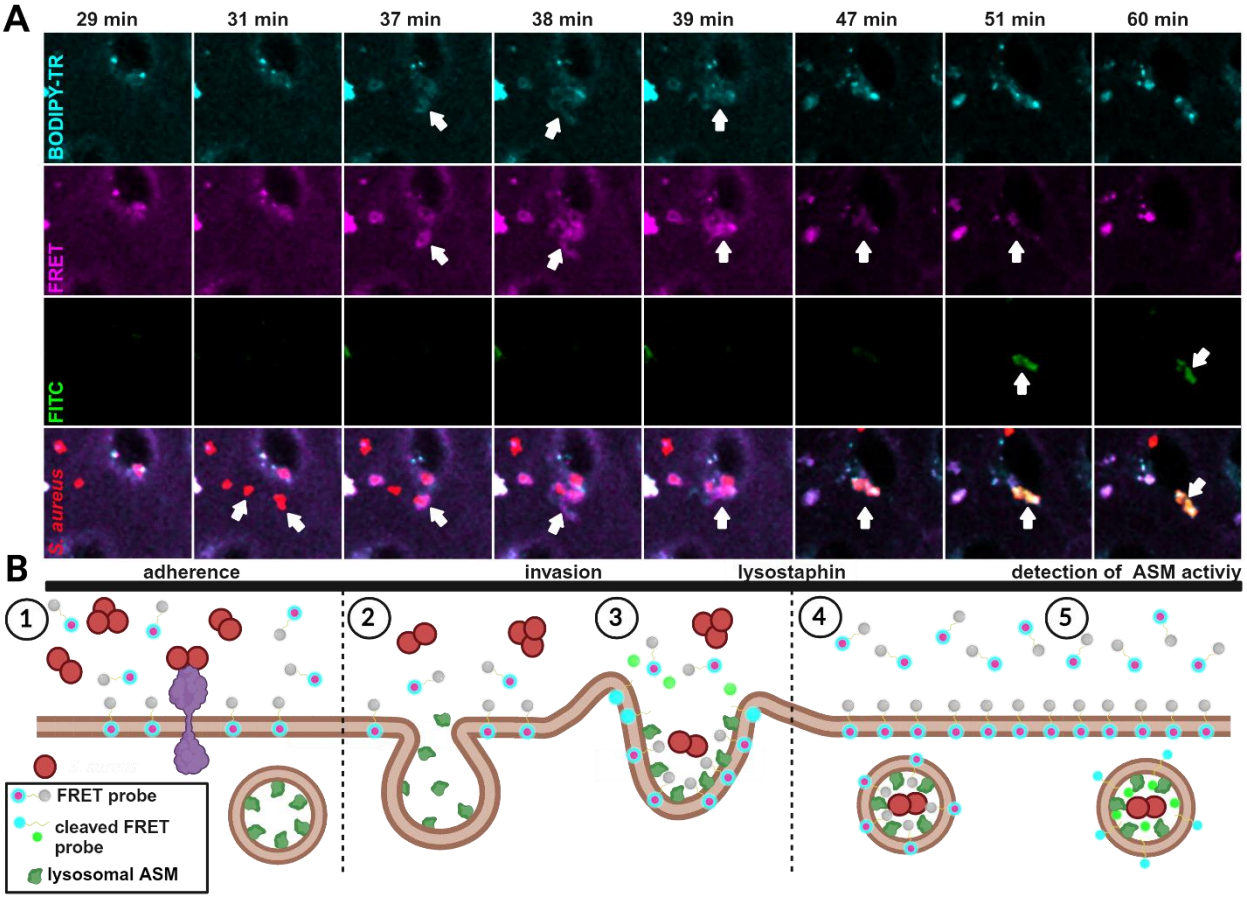

Supp. Figure 4 *S. aureus* associates with a visible-range SM probe during host cell invasion.
(A) Live cell imaging of *S. aureus* infection reveals association of the bacteria with a SM analog during cell entry. HuLEC were treated with 10 µM of a visible range FRET probe in presence of 1% FBS. Then, cells were infected with *S. aureus* JE2 in presence of the probe and infection was monitored by live cell confocal imaging. After 40 min, lysostaphin was added to remove extracellular bacteria. The BODIPY-TR signal demonstrates the localization of the probe, the FRET signal indicates an intact, non-metabolized probe, whereas FITC fluorescence indicates probe cleavage by ASM. Bacteria of interest (white arrows) adhere to host cell between 29 and 31 min p.i. **(B) Hypothetical model of *S. aureus* invasion.** (1). The interaction of bacteria with the host cell surface triggers lysosomal exocytosis, release of ASM (2) and the uptake of the bacteria (cmp. to A: at 37-39 min p.i.) by ASM-dependent membrane remodeling (3). ASM is co-internalized together with bacteria (4) and subsequently, cleaves the probe within the *S. aureus*-containing phagosome (5) (cmp: to A: increasing FITC signal starting at 47 min p.i.).

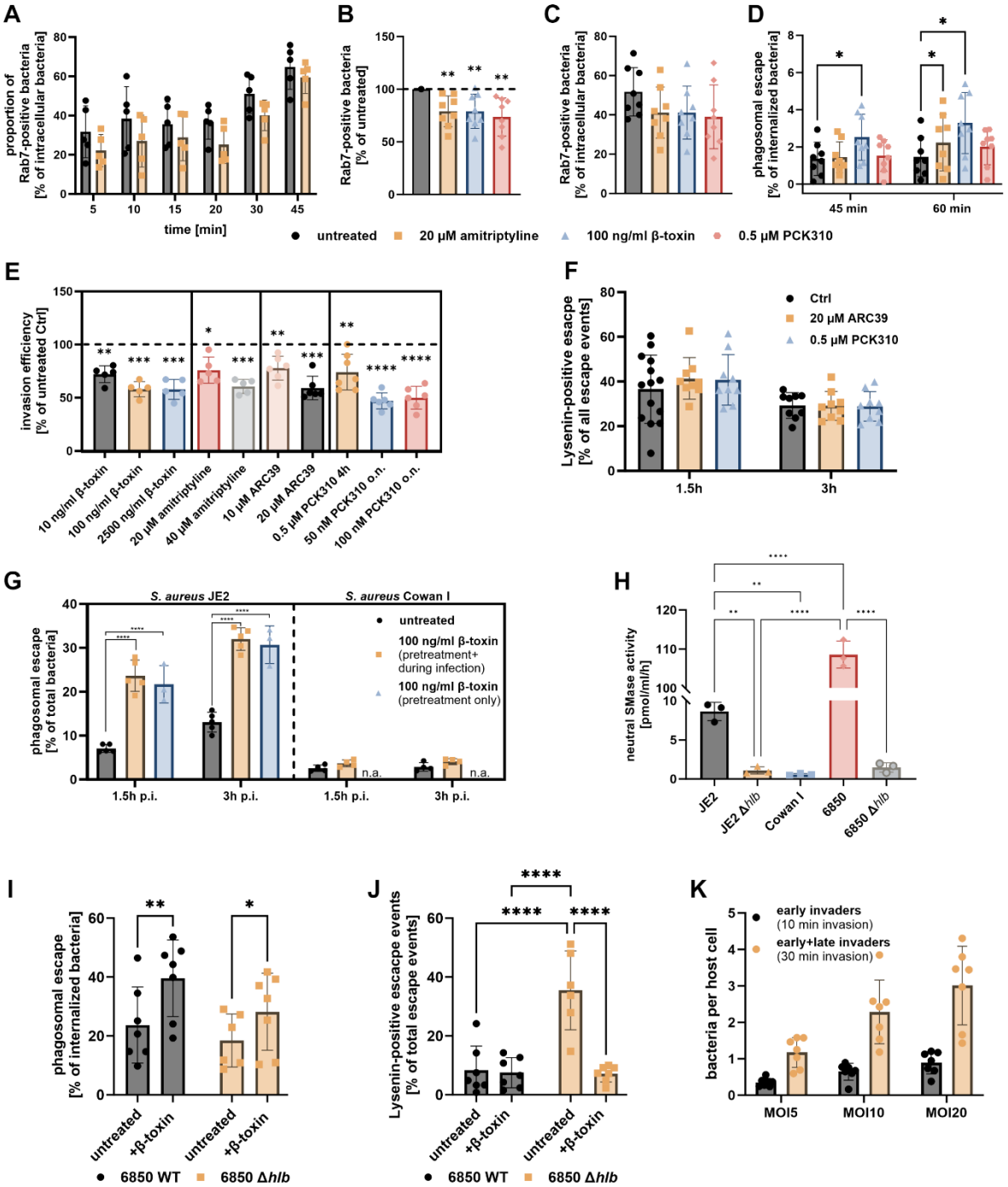

Supp. Figure 5 Supporting information for phagosomal maturation and phagosomal escape measurements.

(A) amitriptyline treatment reduces the proportion of Rab7-positive bacteria. HeLa cells expressing YFP-Rab7 and mCherry-Rab5 were infected with *S. aureus* JE2 for the indicated time point and extracellular bacteria were removed with lysostaphin for 15 min. Then, samples were fixed and imaged by CLSM. Proportion of bacteria associated with YFP-Rab7 was determined. n=5. **(B, C) Reduced association of *S. aureus* with Rab7 is not due to changes in phagosomal escape.** HeLa cells expressing YFP-Rab7 and the phagosomal escape marker RFP-CWT were treated with amitriptyline, PCK310 or β-toxin and subsequently, infected with *S. aureus* JE2 for 45 min and analyzed by CLSMs. Bacteria that escaped from phagosomes were subtracted from the data set and the proportion of residual bacteria associated with Rab7 was determined (C). Results of treated samples were normalized to untreated controls (B, n=7) . **(D) Phagosomal escape assay in early infection.** A HeLa reporter cell line expressing YFP-Rab7 and RFP-CWT was treated with amitriptyline, β-toxin and PCK310 and subsequently infected with *S. aureus* JE2 for 30 min. Extracellular bacteria were removed by lysostaphin and the

proportion of bacteria that acquired the phagosomal escape marker RFP-CWT was determined 45 and 60 min p.i. (n=8). **(E) β-toxin treatment and ASM inhibition reduced invasion efficiency of *S. aureus* JE2 in a dual reporter HeLa cell line.** A HeLa reporter cell line expressing RFP-CWT and Lysenin^{W20A}-YFP was treated with the indicated concentrations of β-toxin and amitriptyline for 75 min, the indicated concentrations of ARC39 for 22 h, 0.5 µM PCK310 for 4h or 50/100 nM PCK310 for 22h (o.n.) and invasion efficiency of *S. aureus* JE2 was determined. (n≥5) **(F) Inhibition of ASM has no influence on the proportion of Lysenin^{W20A}-positive escape events.** The dual reporter cell line was infected with *S. aureus* JE2. Extracellular bacteria were removed and the proportion of bacteria that acquired the phagosomal escape marker RFP-CWT as well as the SM reporter Lysenin^{W20A}-YFP was determined by CLSM. The proportion of escaped (RFP-CWT-positive) bacteria that additionally acquired Lysenin^{W20A}-YFP was calculated. (n=9). **(G) β-toxin pretreatment increases phagosomal escape of *S. aureus* JE2 but not *S. aureus* Cowan I.** RFP-CWT and Lysenin^{W20A} -YFP expressing HeLa were treated with 100 ng/ml β-toxin infected with *S. aureus* strains JE2 or Cowan I. Thereby, β-toxin was either removed prior to infection (pretreatment only) or was present during the whole experiment (pretreatment + during infection). By CLSM, proportions of bacteria that recruited RFP-CWT (phagosomal escape) were determined (n≥3). **(H) *S. aureus* strains vary in β-toxin expression.** The neutral SMase activity in culture supernatants of the indicated *S. aureus* strains or isogenic β-toxin mutants (Δ*hlb*) was determined by a TLC-based approach (n=3). **(I, J) β-toxin pretreatment of host cells but not β-toxin expression of endocytosed *S. aureus* affects phagosomal escape.** HeLa RFP-CWT/Lysenin^{W20A} -YFP were infected with *S. aureus* 6850 or an isogenic strain deficient in β-toxin production (Δ*hlb*). The proportion of bacteria that escaped from the phagosome (I) as well as the percentage of phagosomal escape events that were Lysenin^{W20A} -positive (J) were determined 3h p.i. (n=6). **(K) Increasing the MOI compensates for lower numbers of invading bacteria at shorter infection times.** HeLa cells were either infected for 10 min or 30 min with varying MOIs. Then, the number of intracellular bacteria per host cell was determined 3h p.i. by CLSM. (n=7). Statistics: One samples t-test (B, E), mixed effects analysis (REML) and Dunnett's multiple comparison (D), Two-way ANOVA with Tukey's multiple comparison (G), One-way ANOVA with Tukey's multiple comparison (H), mixed effects analysis (REML) and uncorrected Fisher`s LSD (I), mixed effects analysis (REML) with Šídák's multiple comparison (J).Bars represent mean +/- SD. *p≤0.05, **p≤0.01, ***p≤0.001, ****p≤0.0001.

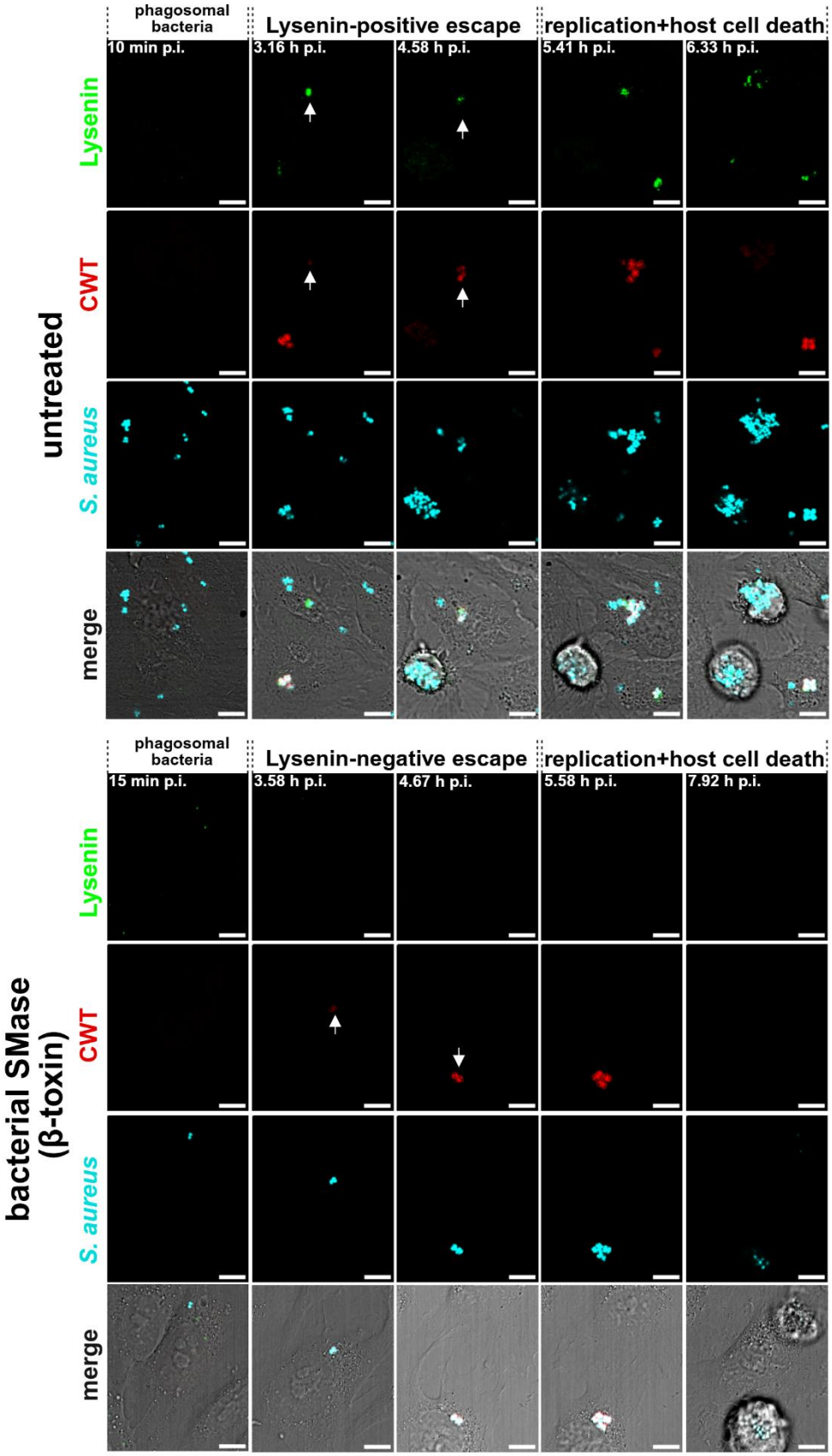

Supp. Figure 6 Validation of Lysenin^{W20A}-YFP and RFP-CWT reporter cell line

Hela cells expressing the SM reporter Lysenin$^{W20A\text{-}YFP}$(green) and the phagosomal escape reporter RFP-CWT (red) were either pretreated with 100 ng/ml bacterial SMase (A) or left untreated (B). Cells were infected with Cerulean-expressing *S. aureus* JE2 (cyan), extracellular bacteria were removed, and intracellular infection was monitored by time-lapse imaging at a Leica TCS SP5 microscope in 5 min intervals. White arrows indicate Lysenin-positive (A)or Lysenin-negative (B) escape events. Scale bars: 10 µm.

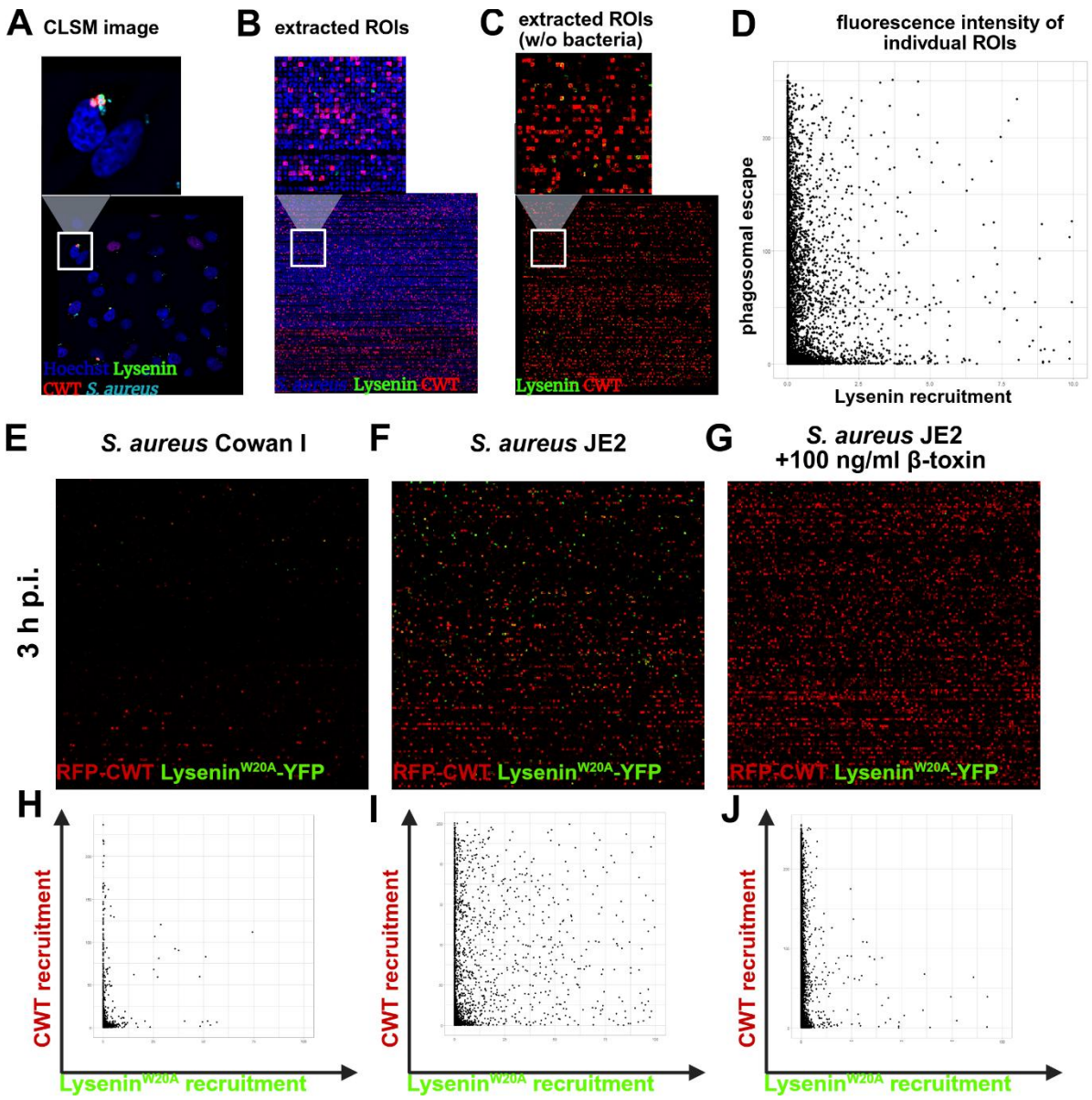

Supp. Figure 7 Evaluation of phagosomal escape and Lysenin^{W20A} recruitment during *S. aureus* infection. HeLa reporter cells expressing RFP-CWT and Lysenin^{W20A}-YFP were infected with *S. aureus* JE2, fixed and imaged by CLSM (**A**). Individual bacteria within the images were identified as regions of interest (ROIs) and extracted in each color channel. All extracted ROIs are depicted in a montage (**B**). If bacteria signals are omitted, the montage of extracted ROIs shows the proportion of reporter recruitment. The average fluorescence intensity of both reporter fluorophores is measured within each individual ROIs is plotted as dot plots (**D**). From these results, the proportion of bacteria that recruited the markers (CWT-RFP = phagosomal escape and Lysenin^{W20A} = SM-rich-phagosome) is calculated. **(E-J) Exemplary escape assay.** Montages of extracted ROIs (without bacterial fluorescence) as well as the resulting intensity measurement in individual ROIs 3 h p.i. are depicted for infections of *S. aureus* Cowan I (E, H) and JE2 (F, I) as well as an infection with *S. aureus* JE2 where host cells were treated with 100 ng/ml β-toxin prior to infection (G, J). Data are quantified in **Figure 5**, B, C.

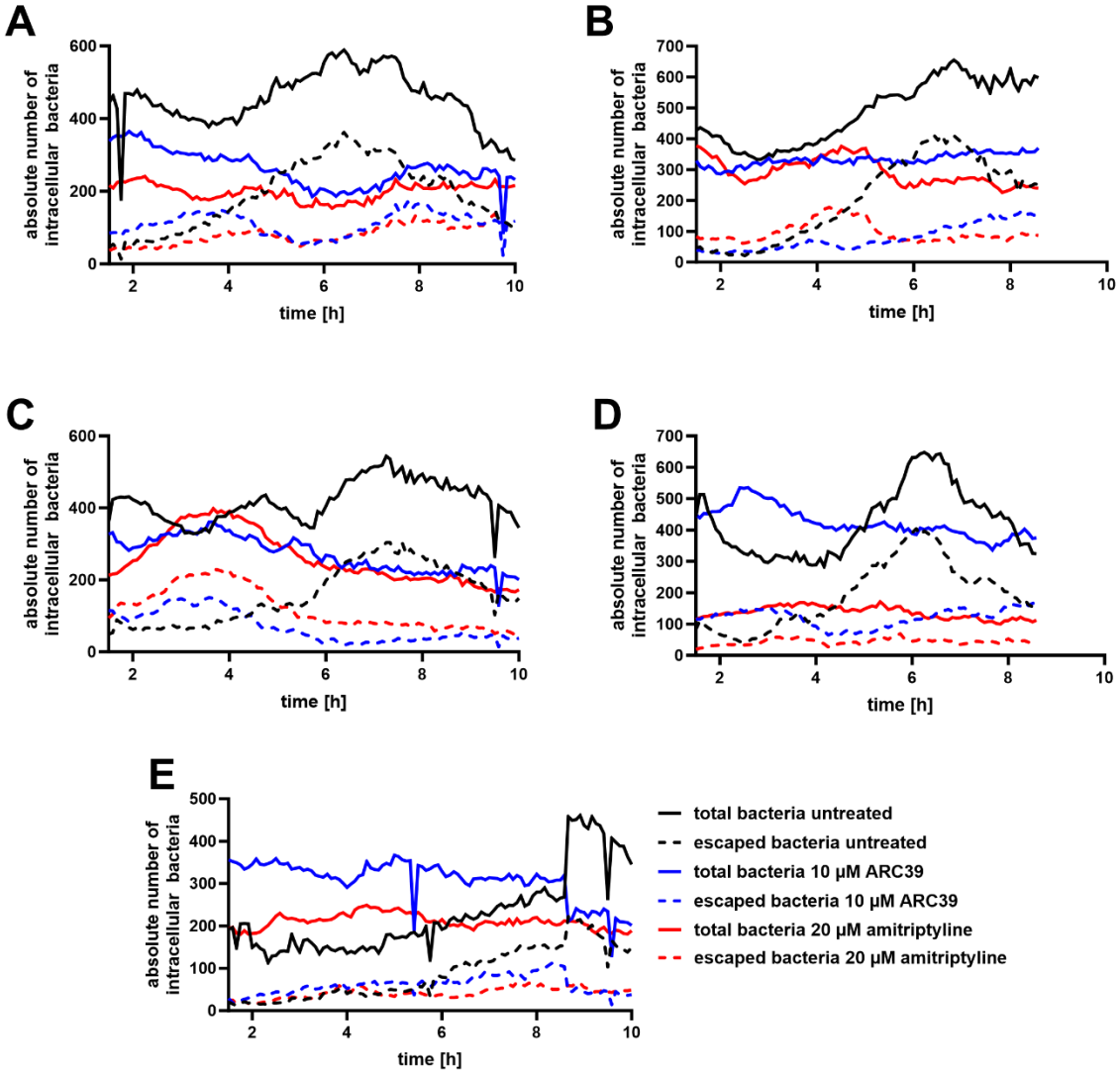

Supp. Figure 8 Individual replicates of time-dependent phagosomal escape and replication assays

HeLa cells expressing RFP-CWT were pretreated with 20 µM amitriptyline or 10 µM ARC39, infected with *S. aureus* JE2 and infection was monitored by live cell imaging (for further details see **Figure 6**, A and B). The absolute numbers of all intracellular bacteria and bacteria that escaped from the phagosome, which were detected during live cell imaging, are depicted.

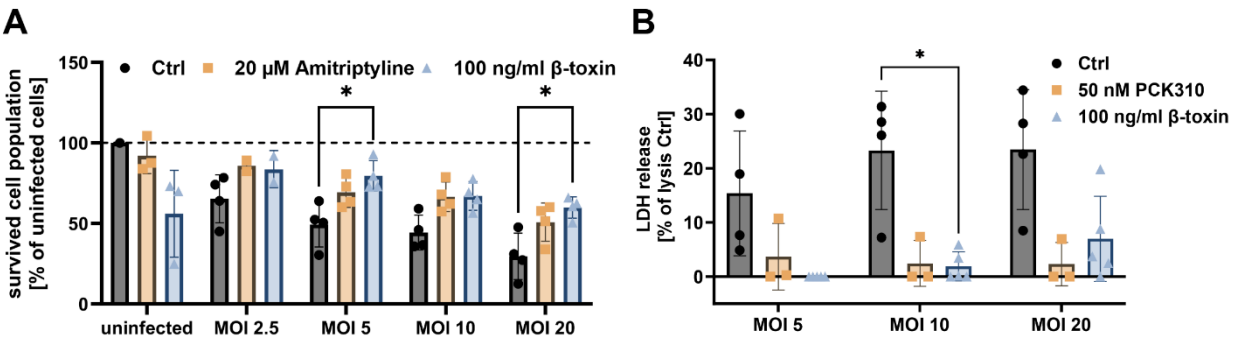

Supp. Figure 9 Inhibition of ASM and β-toxin treatment increase number of host cells remaining attached to the substratum and reduce host cell lysis during infection. HuLEC were treated with amitriptyline or β-toxin (**A**) or PCK310 and β-toxin (**B**) and were then infected with *S. aureus* JE2. After 30 min, extracellular bacteria were removed and the number of cells remaining attached to the substratum was determined (**A**) or the proportion of host cells that were lysed during the infection was measured by lactate dehydrogenase (LDH) release (**B**). Statistics: Mixed-effects analysis and Dunnett`s multiple comparison (A, B). Bars represent mean +/- SD. *p≤0.05, **p≤0.01, ***p≤0.001, ****p≤0.0001.

Supplementary Videos

Supp. Video 1 *S. aureus* associates with BODIPy-FL-C_{12}-sphingomyelin during invasion
(for further details, see Figure 3, A)

Supp. Video 2 *S. aureus* associates with a visible-range FRET probe during invasion
(for further details, see Supp. Figure 4)

Supp. Video 3 *S. aureus* associates with Rab5 and Rab7 upon host cell entry
Hela cells expressing mCherry-Rab5 (red) and YFP-Rab7 (green) were infected with fluorescent *S. aureus* JE2 (cyan). Time-laps imaging was performed at a Leica TCS SP5 microscope in intervals of 45 s. Scale bar: 10 µm.

Supp. Video 4 Validation of Lysenin and CWT reporter cell line
(for further details see Supp. Figure 6)

Supp. Video 5 β-toxin pretreatment protects HuLEC from *S. aureus* infection
(for further details see Figure 6, c)